EES Catalysis

REVIEW ARTICLE

View Article Online
View Journal | View Issue

Cite this: *EES Catal.*, 2026, 4, 11

Exploring the degradation of catalyst layer and porous transport layer in proton exchange membrane water electrolyzers

Shahid Zaman, † Leila Moradizadeh,† Dhinesh Kumar Murugaiah, † Mohmmad Khalid, S. Roohan Farooq Lala and Samaneh Shahgaldi*

Proton exchange membrane water electrolyzers (PEMWEs) are among the emerging technologies for hydrogen production due to their high operational current density, low operating temperature, and ultra-pure hydrogen production. However, industrial scale hydrogen production *via* PEMWEs is greatly hindered by the interrelated trio-factor of low performance, limited durability, and high cost. The iridium-based catalyst layer (CL) and platinum-coated titanium-based porous transport layer (PTL) are the core components which primarily contribute to the performance, durability and cost of PEMWEs. The degradation of costly CL and PTL (due to Ir and Pt usage) is a significant challenge for wider development of PEMWEs. In this review, we discuss the degradation of CL and PTL and provide an overview of the diagnostic techniques used to investigate the degradation processes. *In situ* and *ex situ* analysis reveal that the future development of CL should be focused on ink properties optimization and catalyst coated membrane fabrication methods, which affect the CL architecture and performance. Similarly, the titanium passivation, corrosion and increased interfacial contact resistance are the key factors that affect the PTL microstructure and performance. Thus, it is crucial to develop corrosion resistant coating and incorporation of low-cost materials as interlayers to reduce the cost without compromising the stability of PTL. The understanding of CL and PTL degradation and their characterization methods along with future perspectives will guide the development of durable and low-cost CL and PTL for wider applications of PEMWEs.

Received 9th September 2025,
Accepted 23rd October 2025

DOI: 10.1039/d5ey00270b

rsc.li/eescatalysis

Broader context

The global push toward carbon neutrality has intensified the demand for clean hydrogen production technologies. Proton exchange membrane water electrolysis (PEMWE), when powered by renewable energy, stands out as a promising solution for sustainable hydrogen generation. However, widespread commercialization remains limited by critical challenges related to performance, durability, and cost—collectively referred to as the TRIO-factor. The two of the most cost-intensive and performance-critical components of PEMWE are the catalyst layer (CL) and porous transport layer (PTL). By focusing on their degradation mechanisms, fabrication techniques, and diagnostic tools, this work provides comprehensive insights into extending component lifetimes and reducing overall system costs. Importantly, the review emphasizes the underexplored yet vital role of the CL–PTL interface in cell degradation. This timely contribution aims to guide researchers and industry professionals toward the development of next-generation CL and PTL materials, ultimately accelerating the deployment of PEMWEs for economically viable green hydrogen production.

1. Introduction

Hydrogen produced through water electrolysis serves as an energy carrier, offering the most sustainable solution for a complete transition from fossil fuels to renewable energy. Also, hydrogen as an energy carrier has huge potential to meet the global energy demands, including industrial (steel production, ammonia production, *etc.*), power generation, heating (industrial and domestic), space and automotive applications (aviation, maritime, heavy-duty transportation) due to its high energy density and zero emissions.[1] Electrolyzer technologies, including proton exchange membrane water electrolyzers (PEMWE), alkaline water electrolyzers (AWE), solid oxide electrolyzers (SOEC) and anion exchange membrane electrolyzers (AEMWE), are commonly used for hydrogen production. Among these, AEMWE and SOEC are less mature technologies

Hydrogen Research Institute, Université du Québec à Trois-Rivières, Quebec, Canada. E-mail: Samaneh.Shahgaldi@uqtr.ca
† These authors contributed equally to this work.

with lower technology readiness levels, limited demonstration scales, higher costs and relatively high degradation rates of 1.0 and 1.9 μV per hour, respectively.[2] In contrast, AWE and PEMWE are more established technologies with higher technology readiness levels, demonstrating lower degradation rates of 0.12 μV h^{-1} and 0.19 μV h^{-1}, respectively.[3] While AWEs are known for their long testing durations, noble metal-free electrocatalysts, and proven stability, PEMWEs stand out for their high operational current density (1–3 A cm^{-2}) at low operating temperatures, low voltage losses, higher response times (in milliseconds), ultra-pure hydrogen (99.99%), and superior ionic conductivity. PEMWEs are also well-suited for integration with intermittent renewable energy sources due to its compact design and higher selectivity, making it a highly promising technology for hydrogen production.[4]

Despite the advantages of PEMWE, the high cost of catalysts and the limited stability of cell components remain significant barriers to its widespread adoption.[5–7] Platinum group metals (PGM) are used in catalyst layers (CL) and porous transport layers (PTL) coatings to achieve high performance and stability. However, the use of PGMs significantly increases the overall cost of PEMWEs. Therefore, reducing PGM loading, especially in CL and PTL, is crucial for lowering the overall cost. Yet again, the CL with low Ir loadings and the PTL without noble metal coatings are prone to degradation and surface passivation, respectively, which affect cell performance and stability. Thus, understanding the microstructure of CL and PTL, as well as the factors that affect their performance and stability, is crucial for addressing the high cost and limited durability challenges. The microstructure of the CL plays a critical role, as it directly affects structural integrity, electrical conductivity, and accessibility of active sites. These properties are associated with CL degradation processes such as dissolution, migration, and agglomeration of catalyst nanoparticles. To minimize precious PGM usage while ensuring durability, it is important to modify the microstructure through nanostructure engineering, as simply reducing PGM content could accelerate degradation.[8,9] Likewise, lowering PGM coatings in the PTL may increase interfacial contact resistance (ICR) at the PTL/CL interface due to the formation of an insulating oxide layer. In addition to these challenges, the porous structures of the CL and PTL are affected by the distribution of liquid water and bubble dynamics, which can lead to mechanical degradation. In this review, we discuss the state-of-the-art CL and PTL degradation, highlighting the underlying processes and characterization methods to analyze and mitigate the degradation, followed by future directions for large-scale development of PEMWE at a reduced cost.

2. Catalyst layer

Membrane electrode assembly (MEA) is a core component of PEMWE and constitutes anode and cathode CLs separated by a solid polymer electrolyte membrane made of perfluorosulfonic acid (PFSA). Anode CL consists of iridium (Ir) based catalysts (IrOx) for oxygen evolution reaction (OER) and platinum (Pt) supported on carbon (Pt/C) as a cathode catalyst for hydrogen evolution reaction (HER).[10] HER kinetics at the cathode are extremely fast in acidic conditions, resulting in a negligible overpotential that has a minimal impact on the overall PEMWE performance. However, long-term operation still contributes to cathode CL degradation *via* catalyst dissolution and catalyst detachment from the support, which affects the overall durability of the cell. In contrast, OER kinetics are a complex multistep reaction pathway. It requires the continuous splitting of reactant H_2O and the rapid removal of product O_2 from the catalyst surface (triple-phase boundary) simultaneously.[11] Therefore, anode CL requires a higher Ir loading (1–2 mg_{Ir} cm^{-2}) to facilitate the sluggish OER, accounting for more than 25% of the total stack cost and dictating the overall cell efficiency.[12]

A typical CL is developed from a dispersion-based catalyst ink, which consists of catalyst nanoparticles dispersed in ionomer and solvent. The ink formulation and mixing method substantially influence the interactions among the ink components. The ionomer in the catalyst ink is distributed over the aggregates and agglomerates that form a multiscale porous structure through a coating and drying process known as CL microstructure. Each ink formulation creates a unique microstructure in the CL, resulting in varying porosities (meso- and macro-pores) and plays a crucial role in both reactant flow and the efficiency of catalytic sites. A distinctive proton transport phase is carried out by the ionomer in the CL and reactant water, while the electron transport pathway generally occurs through the catalyst (support)/PTL/current collector interface. Thus, a well-designed microstructure increases the interfacial contact area between CL and the membrane, enhancing the overall reaction efficiency. Similarly, a good interfacial contact between CL–PTL facilitates the transport of product gas that passes through the porous CL and exits through the PTL.[13] Therefore, constraints to any of these transport pathways would directly increase the electrode overpotential, affecting the overall cell performance.[14,15]

2.1. Catalyst layer degradation

The primary degradation mechanisms in CL include the dissolution, migration, and agglomeration of Ir-based catalyst nanoparticles, CL detachment, and support passivation due to harsh operating conditions (low pH and high anodic potential).[16] The OER on the catalyst surface generally proceeds *via* oxide route, where the participation of lattice oxygen atom facilitates efficient OER.[17] However, the lattice oxygen route leads to mechanical stress on the oxide layer of the catalyst, accelerating the dissolution rate.[18] Depending on the applied potential and the surface composition of the catalyst, Ir dissolution is likely to occur through three different dissolution pathways.[19] At lower potentials (<0.9 V), direct dissolution of metallic Ir can occur before the formation of a stable oxide layer (Fig. 1).[20] Specifically, under potentiostatic conditions or during high-scan-rate cycling, the oxide formation lags behind the applied potential. In the intermediate potential range ($\sim$0.9–1.4 V), the Ir surface undergoes redox transitions

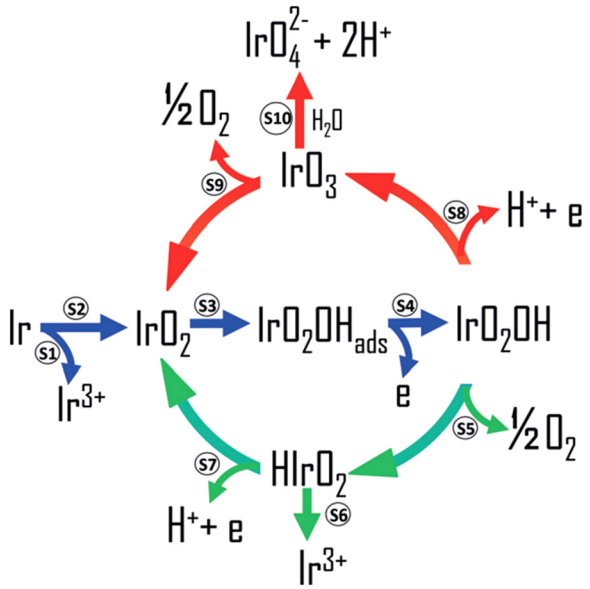

Fig. 1 Simplified scheme showing possible pathways of Ir dissolution. Green arrows indicate the mechanism that is preferable for electrocatalytically active Ir-based materials at lower potentials. Red arrows present the dissolution route dominating at higher anodic potentials. Blue arrows show intermediate steps that take place regardless of the electrode material and potential. Adapted from ref. 22 with permission from Wiley-VCH, copyrights 2018.

involving metastable species such as Ir^V (*e.g.*, Ir^VO_2OH) and Ir^{III} (*e.g.*, $HIr^{III}O_2$), which can either dissolve or transform into IrO_2 through a place-exchange mechanism that replaces surface OH/O species with lattice oxygen. At higher potentials (>1.4–1.6 V), further oxidation leads to the formation of Ir^{VI} species such as IrO_3, a highly reactive and unstable oxide that can decompose into IrO_2 and O_2 or hydrolyze to form soluble IrO_4^{2-}, contributing significantly to catalyst degradation. These mechanisms highlight the complex interplay between redox chemistry, oxide formation, and dissolution that governs the stability of Ir-based catalysts under OER conditions.

In this process, oxygen atoms from water or hydroxide displace surface iridium atoms, embedding oxygen into the lattice and pushing Ir atoms slightly outward, forming a true bulk-like oxide rather than just surface adsorption. This transition begins around 1.0 V and accelerates at 1.2 V. This marks the onset of irreversible structural changes that render the electrode susceptible to further hydration, dissolution, and oxygen evolution at higher potentials.[21] At high potentials, OER accelerates the dissolution of Ir due to the formation of unstable hydrous oxides and high-valent intermediates such as $Ir^{5+}$and Ir^{6+}. This potential region is associated with the most severe degradation, driven by oxide hydration, redox instability, and highly oxidative conditions.[18] However, the mechanism transitioning between Ir^{5+} and Ir^{3+} is considered the dominant dissolution pathway.[22] This dissolution not only leads to catalyst loss but also drives morphological changes in the CL.

The dissolution of Ir significantly influences the aggregation and redistribution of catalyst particles. One such process is Ostwald ripening, in which smaller nanoparticles dissolve into the electrolyte and subsequently redeposit onto larger particles (Fig. 2a). Concentration gradients drive this redeposition and is further affected by local conditions such as pH variations and supersaturation resulting from metal dissolution. At higher overpotentials, coalescence may occur, where nanoparticles collide and merge due to electrochemical energy, forming bigger particles.[23] Furthermore, the dissolved ions migrate to the IrO band in the vicinity of the CL/PEM interface in the MEA, and further migration through the PEM leads to redeposition into Pt–Ir NPs in the cathode (Fig. 2b).[24] An unsupported

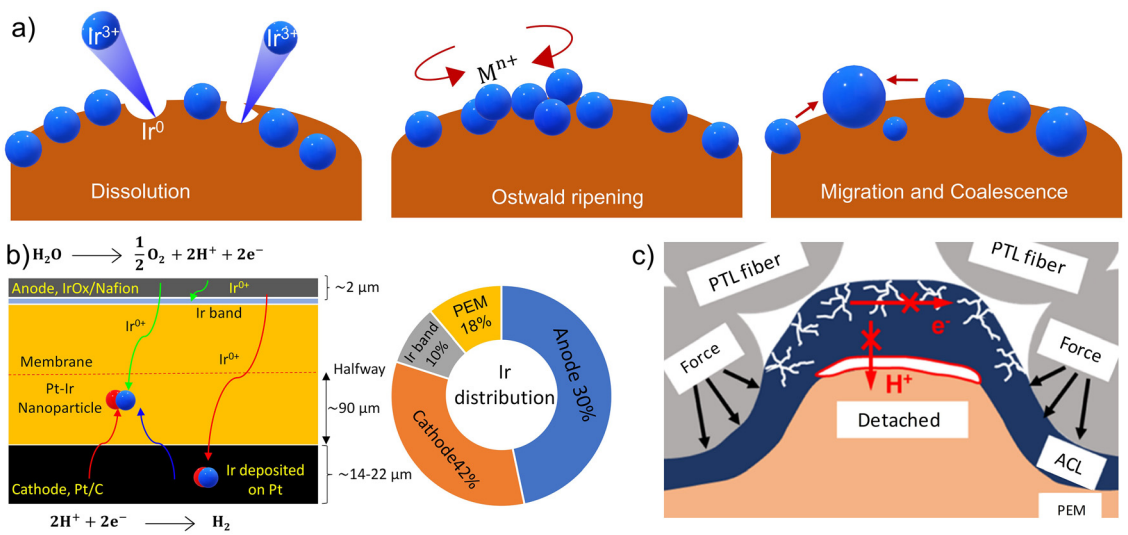

Fig. 2 (a) Schematic of Ir nanoparticle dissolution, redeposition and coalescence. (b) Diagram depicting the mechanism of Pt–Ir precipitates and Ir band formation in the membrane, with the distribution of Pt and Ir at different regions of the MEA. Adapted from ref. 24 with permission from Elsevier, copyrights 2019. (c) Schematic of the mechanical degradation that takes place in the anode CL. Adapted from ref. 33 with permission from American Chemical Society, copyrights 2024.

Ir-based catalyst stands out for its exceptional intrinsic catalytic activity and simplicity, with no risk of support degradation or interference. This makes it ideal for high-performance systems. However, supported catalysts could offer enhanced durability, better Ir dispersion, and reduced Ir loading on a high surface area, making them well-suited for long-term operation under high-current operating conditions and at a lower cost.[25] Carbon-based nanostructural materials are commonly used as catalyst supports in electrocatalysis; however, their corrosion and oxidation under harsh electrochemical conditions render these materials unsuitable for anode catalysts in PEMWEs. In contrast, metal-based supports, such as metal oxides, borides, and nitrides, provide superior corrosion resistance, improved conductivity, and long-term stability, which are more suitable for higher voltage operating conditions of PEWMEs.[26] Titanium oxide (TiO_2), with excellent corrosion-resistant properties, is the only IrO_2-supported commercial catalyst (IrO_2/TiO_2, *Umicore*).[27] Nevertheless, the limited conductivity of TiO_2 needs higher IrO_2 loadings to maintain sufficient conductivity of CL in PEMWEs, which hinders the fabrication of low Ir loading CL.[28] Therefore, using other conductive and corrosion-resistant materials, such as metal oxides and metal borides, can eliminate the need for excess IrOx loading to maintain conductivity due to their inherent high conductivity properties. Therefore, depositing Ir nanoparticles on such a catalyst support could significantly reduce the Ir loadings without compromising durability.[29,30]

Recently, different metal oxide-supported Ir catalysts have been reported as efficient and durable anode catalysts in PEMWEs.[31] For example, IrOx-supported niobium oxide demonstrated exceptional stability as anode CL in PEMWEs due to the dynamic migration of oxygen species between IrOx and Nb_2O_{5-x}.[25] The *in situ* structural analysis revealed that the Ir oxidation state is maintained throughout durability testing due to the spontaneous migration of excess oxygen from IrOx to the Nb_2O_{5-x} support. This stabilizes the active Ir sites, thereby maintaining the catalyst's efficiency over an extended time. Another severe issue is ionomer degradation, which alters the entire CL microstructure, thereby changing the wettability and bubble kinetics. When the ionomer degrades, these crucial interactions are disrupted, leading to a loss of performance, even if the catalyst itself remains stable. Thus, understanding the interplay between the support material and ionomer degradation is key to enhancing the long-term stability and efficiency of PEMWE catalysts. Ionomer degradation generally results in a higher overpotential (decrease in ion conductivity of CL) when metal cations occupy the proton exchange sites of ionomers.[32] Chemical degradation of ionomer typically takes place at a lower cathodic potential, resulting in loss of the triple-phase boundary that increases the activation overpotential at the cathode and ends up with detachment or coalescence of Pt NPs due to weak van-der-Waals forces.[24] Although ionomer degradation in anode CL is less pronounced, it affects wettability and bubble detachment, leading to bubble-induced kinetic and mass transport polarization. Therefore, the bubble coverage in catalyst active sites and the modified pore structure ultimately result in explicit mechanical stress on the anode CL. This results in ionomer depletion and cracking of the CL, leading to a loss in the effective electrochemical surface area (Fig. 2c).[24,32]

Degree of degradation in CLs is also dependent on the operating conditions, such as, constant current hold at low current densities (0.1–1 A cm^{-2}) shows a significantly lower voltage loss as compared to operation at high current densities ($\geq$2 A cm^{-2}).[25,34,35] The increase in overpotential during low current density operation is generally attributed to activation losses due to intrinsic kinetics of the electrode reactions.[36] Over time, these losses may be exacerbated by degradation of the CL or ionomer, particularly at the anode, where high oxygen partial pressure and oxidative species can lead to chemical breakdown. Under high current density conditions, Ir-based catalysts experience dissolution, which results in particle growth or changes in morphology *via* redeposition, migration, and coalescence.[37] Moreover, the low cathodic potential at high current densities promotes the formation of peroxide radicals, contributing to Pt detachment and coalescence due to weaker van der Waals forces.[38,39] CL durability also depends on the nature of the catalyst and the resultant CL architecture. For example, a direct comparison reveals that an unsupported Ir-based catalyst degraded after 208 hours due to surface oxidation, characterized by an increase in electrical resistance (at 1.8 V_{RHE}, 60 °C).[40] In contrast, a CL having low Ir supported nanostructured catalyst support (0.08 mg_{Ir} cm^{-2}) operated for 4500 hours at 1.8 A cm^{-2} and 80 °C due to enhanced active site accessibility provided by a nano-porous ultrathin film electrode.[39,41,42] The modified CL *via* incorporation of IrOx nanofiber interlayers in the anode led to improved surface area and electron transfer, resulting in better mechanical stability and a lower overpotential (14 mV *vs.* 68 mV for nanoparticle-based MEAs) after 4000 cycles at 2 A cm^{-2}.[43]

Under dynamic operation conditions, the frequent removal of bubbles at the catalytic site enhances the water transport and prevents reversible degradation. However, it causes severe CL degradation due to Ir dissolution and ionomer thinning. For instance, operating under load fluctuation, the accelerated rate of bubble formation and detachment results in bubble-induced stress on CL. The accumulation of bubbles on the electrode surface can lead to localized thermal hotspots due to hindered heat dissipation and mass transport. These hotspots induce thermal stress on both the ionomer and catalyst materials in the CL, potentially accelerating degradation.[44] Furthermore, during system shutdown, H_2 crossover leads to a decreased electrode potential at the anode, reducing IrOx to metallic Ir.[10,37] Upon startup, the metallic Ir is re-oxidized to an amorphous Ir, which influences the electrode's performance and stability. Although there is an initial improvement in performance, this is followed by rapid CL degradation due to the dissolution of Ir. This issue could potentially be mitigated by optimizing the operating parameters during the on/off cycle intervals.[18,21,23,45]

2.2. Characterization of CL degradation

It is crucial to understand and visualize the changes in CL microstructure to identify degradation mechanisms. Traditionally,

ex situ characterizations, such as post-durability morphology analysis were conducted to analyze CL after performance testing. However, currently, *in situ* electrochemical analysis, such as real-time voltage loss (voltage loss as overpotential) monitoring and increased high-frequency resistance (HFR), provides valuable information about degradation mechanisms. Fig. 3a illustrates the voltage breakdown in PEMWE, highlighting the voltage contributions from each component. It demonstrates that the anode kinetic losses are the largest contributor to the overall voltage loss. *In situ* electrochemical characterization techniques, such as polarization curves, electrochemical impedance spectroscopy (EIS), and cyclic voltammetry (CV), provide valuable insights into the current–voltage relationship. Mass transport losses are not shown due to the usual insignificant contributions to the overall voltage losses in PEMWEs.[46] These insights help elucidate the underlying reaction mechanisms and increased overpotential.[47] The corresponding polarization curves analysis shows degradation, demonstrating all the losses at the beginning and end of the test (EOT) (Fig. 3b). Generally, the lower current density region is dominated by kinetic overpotential and Ohmic polarization, which

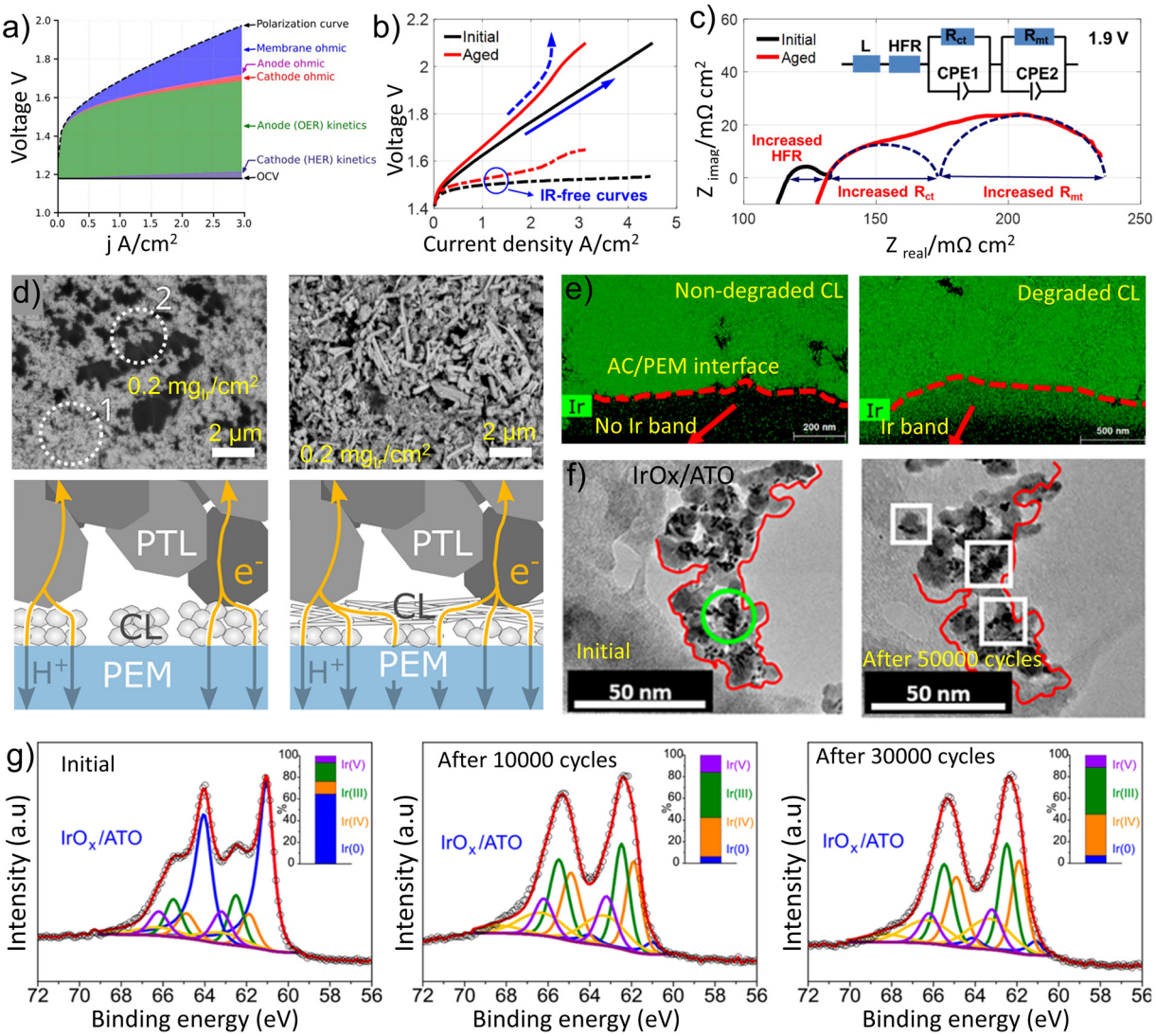

Fig. 3 Characterization of CL degradation. (a) Schematics of voltage losses across the MEA (mass transport losses are considered negligible). Adapted from ref. 61 with permission from American Chemical Society, copyrights 2020. (b) *I–V* curves at the beginning and end of the test, (c) with corresponding PEIS at 1.9 V. Adapted from ref. 33 with permission from American Chemical Society, copyrights 2024. (d) (top) SEM images of low-loaded CL with a representative homogeneous region (1) and some electronically disconnected islands (2) (left). Nanofiber interlayer of the Ir-based hybrid anode CL (right) (0.2 mg_{Ir} cm^{-2}, Nafion-N115) with the corresponding schematic illustration of CL electronically disconnected from PTL and hybrid IrOx anode CL with nanofiber interlayer that distributes electrons to all regions of the CL and enhances stability (bottom). Adapted from ref. 43 with permission from American Chemical Society, copyrights 2020. (e) Comparison of non-degraded and degraded anode CL and the anode/membrane interface with elemental mapping of Ir band. Adapted from ref. 24 with permission from Elsevier, copyrights 2019. (f) Identical location-TEM images of IrOx/ATO as-synthesized and after 5000 cycles, highlighting the degradation during OER, (g) corresponding XPS spectra demonstrating the Ir oxidation over the period of degradation (inset percentage of Ir(0), Ir(IV), Ir(III), and Ir(V)). Adapted from ref. 60 with permission from American Chemical Society, copyrights 2019.

is linearly dependent on interfacial contact resistance, as well as higher current density due to mass transport limitations (effects of bubble dynamics and CL surface porosity). Furthermore, the EIS from Fig. 3c can complement the results from the polarization curve in terms of charge and mass transfer resistance at the electrode and ionic resistance at the membrane interface. CV measurement at intermittent operation provides additional insight into the electrochemically active surface area (ECSA), thereby enhancing the understanding of the kinetics and reaction mechanism at the electrode surface.

In addition to conventional techniques such as polarization curves, EIS, and CV, recent advancements have enabled direct kinetic loss analysis within MEAs. For instance, a hierarchy-configured CCM with embedded voltage sensing wires shows real-time measurement of internal voltages. The data is used to extract the kinetic parameters such as exchange current density and charge transfer coefficients.[48] This technique enable the *in situ* observations of kinetic losses that contribute over 96% to total electrode voltage loss at low current densities, offering unprecedented resolution in characterizing CL degradation. Furthermore, *in situ* EIS measurements at specific MEA locations complement traditional methods by isolating ohmic and kinetic resistances, thereby enhancing degradation diagnostics and catalyst layer optimization. Nevertheless, characterizing the CL through *in situ* single cell measurement does not necessarily provide complete information on degradation.[49] While these *in situ* techniques are employed to analyze the severity of degradation to the CL, a pivotal step in understanding the degradation mechanism is to imitate operational conditions through an accelerated stress test (AST) over a period of 100–4000 hours.[19] While this may seem a fraction of what the actual lifetime operation entails, AST can simulate the increased stress at a single cell level, either for a particular cell component (CL degradation) or overall cell components, specifically under startup and shutdown operations.[50] Startup and shutdown operations can cause thermal cycling and volume changes, inducing mechanical stresses and microcracking. High current densities during startup may lead to overheating and material dissolution, especially at the anode.[51,52] AST focusing on CL degradation is tested by repeated potential cycling or the stepping potential between a region of activity (upper potential limit >1.6 V_{RHE}) and sluggishness (lower potential limit $<$ 1.3 V_{RHE}). In relation to the potential limits, the findings indicate that limited differences are observed for varied upper potential limits (>1.4 V_{RHE}) due to gas blinding of the CL. Testing at this potential range could significantly contribute towards understanding the dissolution mechanism under oxidative conditions.[53,54]

Furthermore, a systematic comparison of various durability protocols including potential holds, triangle- and square-wave cycling, and renewable energy-mimicking inputs shows the role of durability protocols on degradation.[55] For instance, square-wave cycling (1.45–2 V) at 0.1 mg_{Ir} cm^{-2} resulted in a 30% performance loss over 525 hours, with an Ir dissolution rate of 10.2 ng cm^{-2} h^{-1}, compared to 19% loss and 7.1 ng cm^{-2} h^{-1} for triangle-wave cycling. Ramping (potential) profiles revealed that ramp rate also influences degradation, with ramp-up protocol causing 32% loss. Studies showed a constant high current density operation (*e.g.*, 2 A cm^{-2}) lead to significant degradation, up to 194 μV h^{-1} primarily due to Ti-PTL passivation. The contamination of the CL with Ti ions also reduces the anodic exchange current density and increases ohmic resistance.[56] Dynamic cycling, particularly with intermittent pauses or reduced current intervals, can reduce degradation by up to 84% compared to constant operation.[57] Reversible degradation effects, such as voltage recovery after current interruption, account for up to 61% of observed voltage increase. AST protocols simulating renewable energy profiles (wind and solar) showed lower degradation (12–13%) over 90 days but followed similar kinetic degradation pathways.[55] Additionally, open-circuit voltage (OCV) periods accelerate the transformation of crystalline IrO_2 into hydrous iridium oxide, which has lower conductivity and contributes to increased high-frequency resistance (HFR) and interfacial contact losses.[50] Avoiding OCV by applying a small bias (*e.g.*, 1.3 V) during idle periods effectively mitigates degradation. These findings underscore the importance of selecting appropriate AST protocols based on stressor type, severity, and cycling frequency to accurately assess CL and PTL durability. However, an additional *ex situ* postmortem analysis of the CL rationalizes the intensity of underlying degradation resulting from long-term AST.

Microscopic imaging, as an *ex situ* characterization tool provides both quantitative and qualitative assessments of degraded CLs, enabling the identification of structural changes within the CLs. The *ex situ* analysis focuses on observing the morphology, cracks, wettability, and porosity at the EOT, which can provide a qualitative analysis of the CL degradation compared to the beginning of the test (BOT).[24] Generally, the distribution of IrOx nanoparticles in the CL mostly contains regions with a homogeneous coating (region 1) but also certain regions where the catalyst materials are agglomerated and cracked, which are electronically disconnected from the rest of the CL (region 2) (Fig. 3d). A cross-sectional imaging analysis divulges a qualitative analysis of the migration of catalyst nanoparticles from the anode CL to the membrane and further into cathode CL *via* Ir dissolution mechanism.[58] MEA after 4000 h of PEMWE operation shows the dissolution of Pt and IrOx, where IrOx is distributed across the MEA with a distinct IrOx band at the anode CL/membrane interface (10% IrOx) while retaining just 30% of IrOx in the anode. However, 40% of the IrOx was found to be deposited in the cathode, and 18% migrated to the membrane.[24] Such significant catalyst migration and redeposition in the membrane results in increased ohmic resistance, reduced mechanical integrity, and potentially higher gas crossover.

Ex situ characterization can be extended to detect ionomer aggregates that have dissociated from the catalyst surface. This dissociation leads to void formation within the CL, contributing to structural degradation. The dissociated ionomer and migrated catalyst particles can be visualized using scanning electron microscopy (SEM) combined with energy-dispersive

X-ray spectroscopy (EDS). These techniques enable spatial tracking of catalyst migration across the CL and into the membrane. This is illustrated in Fig. 3e, where the Ir signal is shown along the CL/membrane interface. A more obvious degradation *via* identical location transmission electron microscopy (TEM) shows the degradation of catalyst support (marked with red lines), catalyst dissolution/redeposition (green circles) and crystalline migration (white boxes) after 5000 AST cycles (Fig. 3f). X-ray photoelectron spectroscopy (XPS) provides more information on the ionomer in CL, such as the interaction of the ionomer with the catalyst, the conformal state of the ionomer (F : S ratios), and the oxidation of Ir over the course of the degradation period.[59] The fresh IrOx/ATO CL contains a collective of metallic Ir, Ir(III), Ir(IV), and Ir(V) species, which changes to Ir(III), Ir(IV), and Ir(V) species after AST cycle demonstrating the oxidation of Ir, that potentially leads to Ir dissolution pathways (Fig. 3g).[59,60]

3. Porous transport layer

PTL is an essential multifunctional component of PEMWEs that facilitates electron conduction between CL and the bipolar plate (BPP) while managing water and gas transport at the CL/PTL interface.[62] PTL also dissipates the heat produced during PEMWE operation and provides mechanical support to the CL, facilitating the removal of O_2 gas to prevent mass transport losses. Thus, a better functional PTL requires high porosity, conductivity, mechanical strength, and chemical stability in acidic media.[63] Currently, titanium (Ti)-based substrates are used as PTL due to their high electrical conductivity, sufficient corrosion resistance, and mechanical strength.[64] Metallic Ti felt, sintered Ti powder, and Ti mesh are among the commonly used commercial PTL substrates, ensuring effective water and gas transport for the extended applications of PEMWEs.[65,66] However, corrosion, passivation, or mechanical damage of Ti due to bubble formation and compression can increase resistance, limit reactant access, and cause uneven current distribution, thereby accelerating PEMWEs degradation.[67,68]

3.1. Porous transport layer degradation

PTL degradation usually occur through chemical degradation which primarily results from the corrosion, passivation, and poisoning of Ti and mechanical degradation which is mainly driven by the formation of O_2 gas bubbles and compression.[67] Chemical degradation initiates as Ti develops a thin, corrosion-resistant oxide layer when exposed to O_2 or moisture (Fig. 4a).[69]

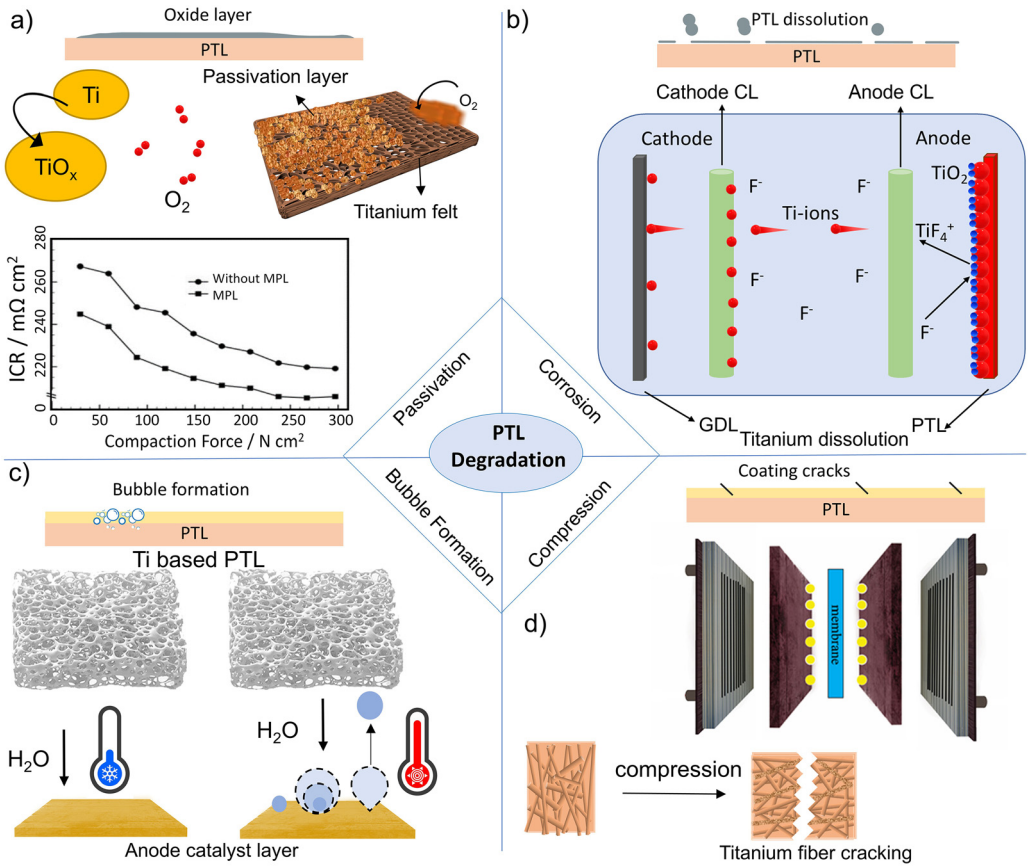

Fig. 4 Illustration of PTL degradation process in PEMWEs, (a) Schematic illustration of PTL surface passivation. Adapted from ref. 89 with permission from Elsevier, copyrights 2016. (b) Schematic of corrosion mechanism and Ti PTL dissolution. Adapted from ref. 63 with permission from Elsevier, copyrights 2025. (c) Schematic of bubble formation and progression to detachment, (d) Schematic demonstration of mechanical degradation of PTL due to excessive compression force.

This oxide layer, due to its electrostatically insulating properties, results in significant interfacial contact resistance (ICR) at the PTL/CL interface, which hampers electron transfer and leads to higher cell resistance.[50] Empirical evidence suggests that after 1000 hours of operation at 80 °C, a 20% increase in ohmic resistance is attributed to the ICR due to the passivation film, resulting in 194 μV h^{-1} voltage losses.[67] This demonstrates the significant contributions (~78%) of anodic PTL to PEMWEs' performance degradation. Thus, a thin layer of PGM (Pt, Ir, or Au) is generally applied to prevent PTL passivation, which minimizes the ICR at PTL/CL.[70] For instance, Ir-coated Ti PTL reduces ohmic resistance by 60 mΩ cm^{-2} and cell voltage by 80 mV compared to uncoated PTL. When operated at a current density of 2.0 A cm^{-2}, the Ir-coated Ti PTL achieved a steady performance for up to 4000 hours without significant voltage losses.[71] Similarly, coated PTL maintains current densities throughout the 4000 h testing period at 2.0 V, which implies that the Ir coating shields the underlying metal from corrosive environments.[65] However, the application of PGM as protective coatings on PTLs significantly contributes to the high cost of hydrogen production in PEMWEs. Although various non-PGM alternatives have been explored, their long-term durability remains insufficient.[63]

Recent advancements indicate that incorporating an interlayer between the PTL substrate and the precious metal top layer can effectively reduce the noble metal loading without compromising performance.[46,72] For instance, the impact of tantalum (Ta) interlayer thickness on PTL performance revealed impressive performance in terms of low Pt loadings. The PTL with a 320 nm Ta interlayer and only 50 nm of Pt achieved a 33% higher current density at 2.0 V compared to a commercial PTL with 200 nm of Pt, thus reducing the PGM usage by a factor of four.[73] Fig. 4a also presents the ICR results of coated and uncoated PTLs under varying compression forces, where a significantly low ICR is observed for coated PTL, which emphasizes the role of thin coatings on PTL in preventing surface passivation.

Catalyst poisoning due to Ti dissolution through electrochemical reactions is another major cause of degradation in PEMWEs.[58] Under high anodic potential (1.4–2.0 V), metallic Ti is susceptible to oxidation, forming TiO_2 and TiO_2^+. These ions further react with fluoride ions (F^-), often present in the system (from membrane degradation or ionic phase) to form soluble Ti-fluoride complexes (TiF_4^+) (Fig. 4b). Which then migrate through the ionomer proton transport channels to the cathode, driven by the electric field and replace protons (H^+) in the ionomer or deposit on the CL. This process disrupts the proton transfer efficiency and can block active sites in CL, thereby hindering HER.[74] Except for PGM coatings that prevent Ti dissolution, the effective removal of F^- and Ti^+ in water loops could also significantly enhance electrolyzer durability, as demonstrated by recent work. A low-cost ion-exchange resin has been utilized in the water loop to remove foreign ions, resulting in a 71% reduction in the degradation rate over a 3000-hour testing period. This highlights the importance of corrosion and poisoning management in improving PEMWE longevity.[74]

The flow of feed water and O_2 gas (bubble formation) has a substantial impact on the mass transport characteristics through the CL/PTL interface. A smooth exit of O_2 gas bubbles generated at the anode CL typically progresses through three stages: nucleation, growth, and detachment.[75] If not removed quickly, bubble formation may hinder the flow of reactants and products, resulting in the obstruction of active sites and disruption of thermal management (Fig. 4c).[76] Thus, it is an essential feature of a good PTL to efficiently distribute liquid water to the CL and facilitate the removal of O_2 gas. This phenomenon is particularly severe under high current densities, where rapid bubble formation creates insulating films at the PTL/CL interface and clogs the micropores of PTL, thereby impeding mass transport.[77] The excessive bubbles may lead to increased local pressure, resulting in structural deformations, cracking, or delamination, particularly in PTL with inadequate robustness. Additionally, the buildup of an O_2 gas concentration gradient near the CL, due to restricted mass transport, decreases the rate of OER.[78] In addition to filling the gaps in CL, a higher concentration of O_2 gas accelerates the phase transition from a dissolved to a gaseous state.[79] This would also disrupt the local pH and concentration gradients, affecting reaction kinetics and raising the risk of localized corrosion or degradation of CL.[80] Similarly, from a thermal management standpoint, O_2 gas has a significantly lower thermal conductivity compared to liquid water, which raises the thermal resistance. This causes 'hot spots' in regions of higher current density due to the Joule effect and accelerates membrane degradation if not adequately dissipated by circulating water or heat conduction.[81] Likewise, such localized overheating contributes to PTL degradation, further compromising PEMWE performance. Various strategies can be employed to facilitate the smooth exit of gas bubbles, including the use of magnetic fields, ultrasound, gravity, and mechanical vibrations, as well as designing and modifying the PTL porosity and wettability.[82–84]

Furthermore, wettability plays a critical role in promoting efficient gas bubble detachment from the PTL surface. Enhanced hydrophilicity of the PTL improves water transport and mitigates bubble accumulation, thereby reducing mass transport losses.[85] The progression of bubble formation and its effects, such as reduced mass transport and increased temperature, are illustrated in Fig. 4c. Furthermore, appropriate compression is essential to prevent water and gas leakage to prevent flooding or dry spots and better contact between CL and PTL to maintain a low ICR. However, the mechanical stability of the PTL, particularly the PTL with high porosity (70–80%), is prone to deformation under excessive compression during cell assembly, due to its porous structure lacking sufficient mechanical strength. This vulnerability can lead to pore collapse or structural damage, impairing gas and water transport.[86] The rib-channel structure inherent in the BPP introduces nonuniform pressure distribution on the PTL, resulting in nonuniform structural changes, which reduce gas and water permeability of the PTL.[87] Excessive compression can also cause Ti fibers to break or shift, altering the structural

morphology and impacting current transport and fluid permeability (Fig. 4d).[88] Furthermore, a PTL fiber crack may puncture the membrane and damage the CL.

3.2. Characterization of PTL degradation

Characterizing the degradation of the PTL is crucial for understanding the underlying degradation mechanisms. Since PEMWE degradation involves contributions from various cell components, isolating the PTL degradation behavior remains challenging, necessitating advanced and targeted diagnostic methods. PTL degradation is commonly characterized by *ex situ* microscopic and structural analysis, electrochemical methods, X-ray techniques and advanced imaging.[72] Microscopic characterizations help to visualize the surface and subsurface characteristics, while electrochemical analysis aids in diagnosing the PTL behavior during the PEMWEs operation.[80,90] SEM allows for direct observation of surface morphology changes, such as cracks, delamination, and coating erosion, arising from mechanical compression and chemical corrosion. For instance, the corroded surface of Ti-based PTL can be observed when exposed to a corrosive environment (Fig. 5a).[72,91] Coupled with EDS, SEM can further identify elemental distribution changes across the PTL, revealing corrosion, essential for pinpointing degradation initiation sites.[92] Microstructural variation is further illustrated by pristine and aged Au-coated PTLs, where Ti fibers, after long-term PEMWEs operation, induced coating delamination (Fig. 5b).[65] Interestingly, the PTL surface at PTL/CL shows complete dissolution of the coating compared to the PTL/BPP interface, presumably due to the formation of an unstable oxide layer. The oxide layer disintegrates at high voltage (2.0 V), releasing O_2 gas and detaching the coating layer, thereby initiating Ti passivation or corrosion. A TiO_x layer (~7 nm, pink) is evidenced on the pristine PTL after 4000 hours on the aged PTL compared with the pristine PTL (Fig. 5c and d). In short, TiO_x is both a symptom and a driver of degradation: it thickens and becomes more insulating over time, while localized dissolution and O_2 bubble nucleation undermine adhesion, jointly triggering passivation and corrosion of the Ti substrate.

PTL surface chemistry and oxide formation can be assessed by XPS to quantify the thickness and nature of Ti oxides formed on PTLs.[93] For instance, PTL after AST has shown a significant increase in the oxide-to-metal ratio, highlighting the impact of prolonged exposure of Ti PTL to acidic conditions. The initial Ti(IV) oxide layer becomes thinner in the pristine PTL, with an oxide-to-metal ratio of around 12.73 : 1, which increases significantly (from 20.82 to 23.7 : 1) due to substantial Ti oxidation under corrosive conditions (Fig. 6a).[94] It is worth noting that Ti

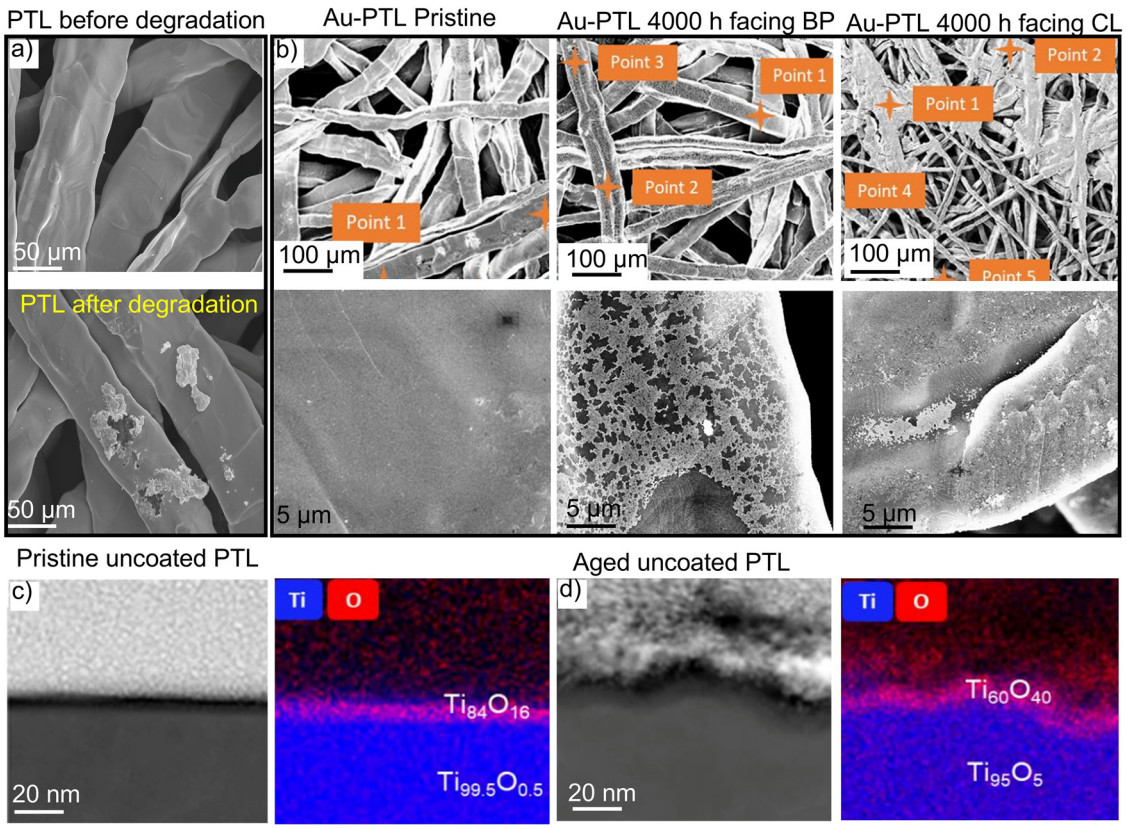

Fig. 5 PTL degradation and characterizations, (a) SEM images of PTL before and after degradation. Adapted from ref. 72 with permission from Elsevier, copyrights 2018. (b) SEM images of pristine Au-coated PTL; Au-coated PTL that faces the BPP and CL side after 4000 h. (c) High-angle annular dark-field scanning TEM images of pristine uncoated PTL and (d) aged uncoated PTL (left), along with elemental distribution (right). Adapted from ref. 65 with permission from Wiley-VCH, copyrights 2021.

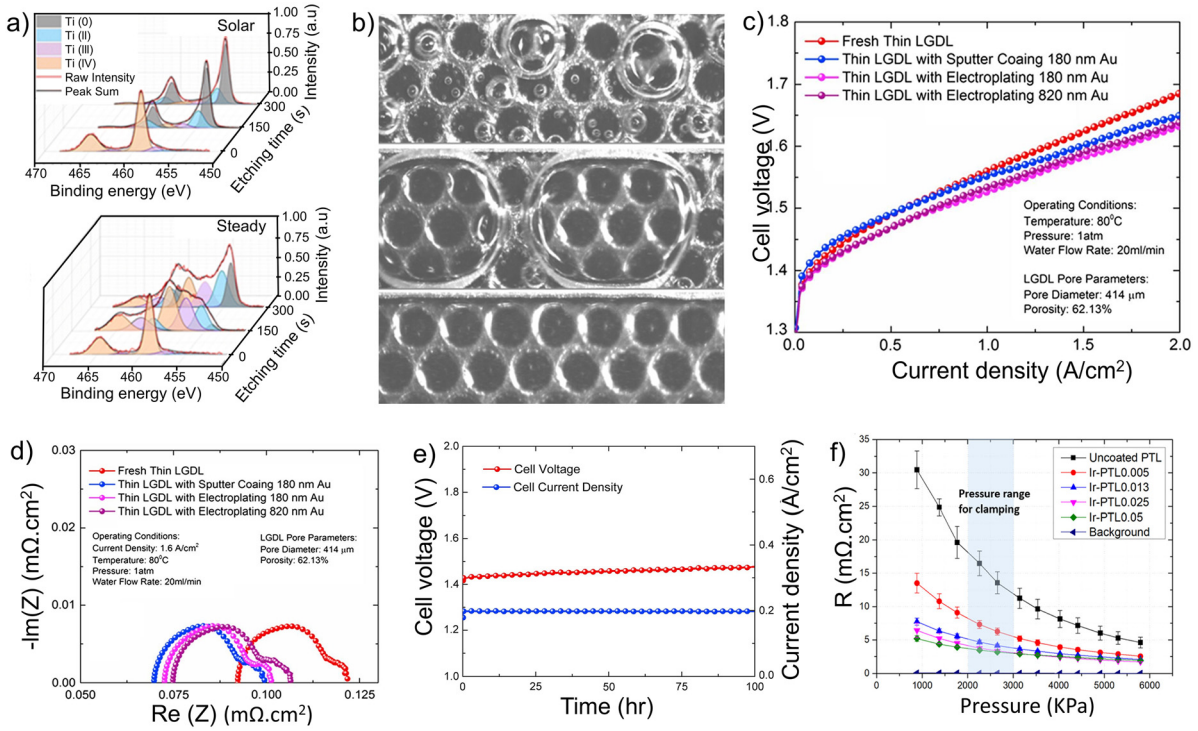

Fig. 6 PTL degradation and characterizations, (a) curve-fitted XPS spectra of fresh and etched under solar and steady AST profiles. Adapted from ref. 80 with permission from Royal Society of Chemistry, copyright 2023. (b) Three flow patterns in the microchannel in the GDL cell and the Ti-felt PTL cell using a neutron imaging technique. Adapted from ref. 98 with permission from Elsevier, copyright 2021. (c) Polarization curve of different PTLs at 80 °C and 0.5 mol L^{-1} H_2SO_4: (d) EIS and (e) potentiostatic polarization curve of Au-coated and uncoated PTL. Adapted from ref. 99 with permission from Elsevier, copyright 2017. (f) Interfacial contact resistance Ir-coated and uncoated PTL. Adapted from ref. 100 with permission from American Chemical Society, copyright 2021.

PTL oxidizes to varying degrees depending on the conditions. For example, degradation analysis during steady operation thickens the oxide layer owing to trapped oxygen in the pores, but dynamic cycling improves gas escape, resulting in a thinner oxide layer. X-ray diffraction (XRD) further reveals phase transitions, indicating that surface oxidation during the degradation process results in new crystal phases, such as TiO_2 and Ti_2O_3 (for Ti PTL), which are generally passive in nature and increase the ICR.[92]

Synchrotron X-ray radiography and neutron imaging enable the real-time observation of PTL degradation by tracking the progression of corrosion. These techniques can also help in studying the bubble formation under operational conditions, providing insights into structural integrity and mass transport dynamics as they evolve.[95,96] Neutron imaging, with its ability to penetrate metal layers, visualizes the distribution of water and gas, thereby aiding in the understanding of bubble formation and transport mechanisms. These *in situ* techniques are crucial for identifying degradation pathways that impede PTL efficiency and enable precise adjustments in PTL design.[97] A recent study reported the relationship between bubble transport and PEMWE electrochemical performance by integrating a visualization window on the anode endplate to observe tailored PTL bubble movement (Fig. 6b).[98] The authors demonstrated that PTL pore architecture dictates bubble detachment and release pathways, where optimized structures promote faster bubble removal, reduce mass transport resistance, and enhance cell performance.

Electrochemical diagnostic could also provide insights into PTL degradation, where the current response to increasing voltage is measured. It defines oxidation onset points and indicates the corrosion susceptibility as well as the impact of the coating layer on the PTL. For instance, uncoated Ti-felts exhibited a voltage of 1.685 V at 2.0 A cm^{-2} and 80 °C, which was reduced to 1.649 V with sputtered Au and further reduced to 1.633 V and 1.638 V for 180 nm and 820 nm electroplated layers, respectively (Fig. 6c).[99] Changes in charge transfer resistance and mass transport impedance at the electrode–electrolyte interface, due to passivation layer formation, raise ICR and undermine PTL functionality. Based on Fig. 6d, the Au coatings reduced ohmic resistance in comparison to uncoated PTL, with the lowest resistance (70 mΩ cm^2) observed for the 180 nm thick Au sputter-coated PTL. Potentiostatic testing, conducted over extended periods, monitors the decline in corrosion current, providing insight into PTL durability under PEMWE conditions. The sputtered (180 nm) and electroplated (180–820 nm) Au-coated Ti-felts improved stability and reduced voltage at 2.0 A cm^{-2} and 80 °C, with electroplated layers showing minimal voltage decay over 100 hours (Fig. 6e).[99] These methods capture shifts in electrochemical stability, which is vital for assessing the integrity of PTL coatings and their functional lifespan.[100,101] These findings highlight Au's

effectiveness in enhancing the stability and performance of PTL. ICR serves as an indirect metric for evaluating PTL degradation, specifically surface passivation. This phenomenon occurs as an insulating oxide layer forms on the PTL surface under PEMWE operation, impeding electron transfer and resulting in increased voltage losses. Fig. 6f presents the ICR results for different Ir coating thicknesses on the PTL across various compression force ranges, where ICR decreased with increased coating thickness, indicating the benefit of thick Ir coatings.[100] Comprehensive analysis of PTL degradation provides crucial insights into the mechanisms driving performance loss in PEMWEs. These findings underscore the need for optimized PTL materials and coatings that withstand harsh electrolyzer environments, promoting stable electron transport and minimizing interfacial resistance.

Most *in situ* studies have been performed under steady-state operation or simplified ASTs protocols. While valuable, such protocols cannot fully reproduce the stresses experienced in real applications, particularly when electrolyzers are directly coupled to intermittent renewable energy sources. In practice, dynamic operation imposes frequent current ramps, start/stop cycles, and rest intervals, all of which accelerate unique degradation pathways that are often absent in steady-state testing.[102] A study on PEMWE testing protocols shows that steady or overly simplified ASTs can misrepresent field degradation if they neglect dynamic cycling and intermittent loads.[102] To obtain representative insights, *in situ* characterization must therefore be adapted to account for realistic load profiles and transient operating states. Recent studies demonstrate that compared to steady testing, dynamic cycling results in increased fluoride release from ionomer/membrane, significant Ir and Pt migration into the membrane.[103] Dynamic testing protocols also evidenced a thin but detectable PTL passivation layers ($\sim$0.4 nm), and partial recovery of activation overpotential during rest periods. These results highlight the vulnerability of the CL–PTL-membrane junction under realistic cycling and highlights the importance of *in situ* studies to capture the exact degradation. Another study further showed that the frequency of dynamic loading is also critical.[104] High-frequency cycling reduces transient overpotentials and mitigates the degradation per cycle. Whereas low-frequency cycling allows prolonged exposure to extreme conditions, promoting bubble accumulation, interfacial stress, and more severe PTL passivation. Together, these results illustrate that not only the shape but also the timescale of the applied load profile governs degradation kinetics.

4. Role of CL/PTL interface

The interface between the CL and the PTL represents a critical junction in PEMWEs, where electrochemical reactions, mass transport, and mechanical stresses intersect. This region directly governs charge transfer and catalyst utilization, particularly under low Ir loadings (<0.1 mg_{Ir} cm^{-2}), where CL/PTL interface quality becomes the dominant factor in overall performance. Ir utilization in the anode CL is strongly affected by the surface properties of the PTL rather than its bulk characteristics. This behavior arises from two main factors: (i) the poor electronic in-plane conductivity of typical CLs, caused by the disruption of their electronic percolation network, and (ii) localized mass-transport limitations beneath PTL contact points within the porous CL.[105] Uneven or coarse PTL surfaces can deform the CL, generate microcracks, and increase activation, ohmic, and mass-transport overpotentials. The fraction of catalyst effectively connected to the PTL determines the degree of catalyst utilization (Fig. 7a–d).[106] Regions lacking electronic contact remain electrochemically inactive, while optimized surface coatings and microporous interlayers enhance the effective contact and facilitate electron transfer.[106] Tailoring the PTL structure by sintering Ti powders with graded pore sizes can enhance the interfacial contact and minimize the mass-transport losses by approximately 60 mV. Uneven or coarse PTL surfaces can deform the CL, generate microcracks, and increase activation, ohmic, and mass-transport overpotentials. Similarly, electron-beam-melted Ti meshes provide more uniform contact and higher catalyst utilization compared to woven meshes.[107] These observations collectively emphasize that maximizing the effective interfacial contact area between the CL and PTL is essential for efficient catalyst utilization, reduced local transport resistance, and enhanced electrochemical stability. Optimized coatings through nanostructure engineering can enhance the performance while reducing the PGM loadings (Fig. 7e). Development of gas diffusion electrodes integrated with PTL is another vital strategy to improve the interfacial conductivity, water bubble dynamics and reduce the overall PGM loadings.[108] A recent work showcased a thin catalyst-coated liquid/gas diffusion layer design where Ir coatings are applied on PTLs as the catalyst, eliminating the need for the anode CL as CCM. Their findings shows superior performance of these specially designed electrodes compared to conventional system and proved to be effective specifically for low Ir loadings. Such smart designs not only improves the CL/PTL interfacial properties but also controls the bubble dynamics and Ir loadings.

In summary, the CL–PTL interface is not a passive boundary but an active, multifunctional region where electronic, mechanical, and degradation phenomena converge. Thus, an optimized interface could facilitate the minimal PGMs loading while maintaining high effectiveness and efficiency. Rational engineering of this interface-through optimized morphology, tailored surface structuring, and controlled porosity is critical to reducing interfacial resistances, enhancing catalyst effectiveness, and suppressing failure pathways that ultimately compromise the durability of the entire MEA.

5. Future perspectives

Both CL and PTL are essential components that not only play a major role in performance but also contribute significantly to the overall cost of PEMWEs due to PGM catalysts and coating

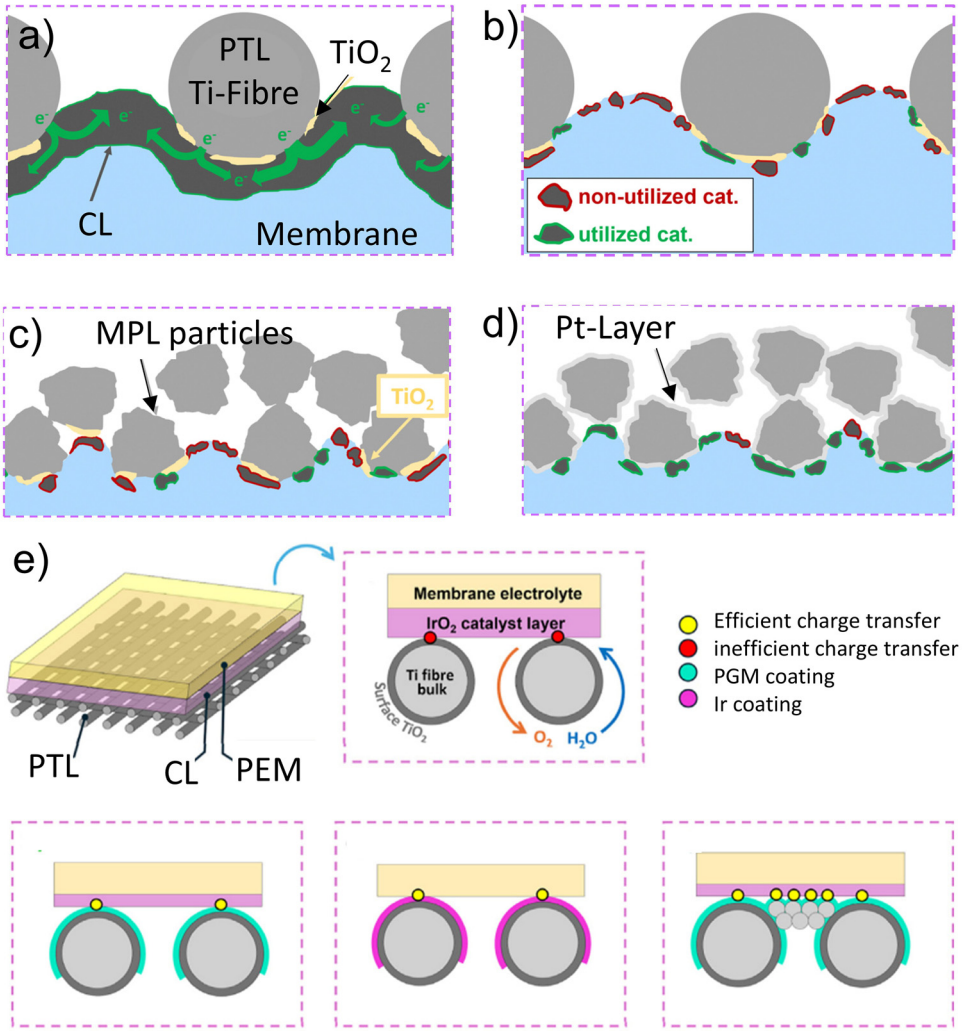

Fig. 7 Schematic illustrations showing the influence of MPL on higher utilization of the CL at low iridium loadings in comparison to that of PTLs and the influence of Pt-coatings. (a) PTL with a CCM using high catalyst loading, (b) PTL with low catalyst loadings, (c) MPL without Pt with low catalyst loading, and (d) MPL with Pt-layer and low catalyst loading leading to better CL utilization. Adapted from ref. 106 with permission from Royal Society of Chemistry, copyright 2024. (e) Schematic illustration of CL/PTL interface modifications and their impact on charge transfer and PGM utilization at the CL/PTL interface. Adapted from ref. 109 with permission from Elsevier, copyright 2024.

on PTL. Therefore, it is essential to understand the degradation process of CL and PTL and design strategies to mitigate degradation for the extended performance of PEMWEs. Following are key points to optimize the CL and PTL for improved performance (Fig. 8).

5.1. Ink optimization

Optimizing catalyst ink can play a key role in enhancing the development of the CL microstructure, which reflects on the durability and performance of PEMWE. Key macroscopic properties of the catalyst ink, such as viscosity, surface tension, material composition, and dispersion stability, should be tuned for better coating. These factors significantly influence the coating process and are essential for reducing the PGM loadings while improving the stability of the CL. The microstructure of CL is not only shaped by its inherent material properties but is also heavily influenced by the fabrication methods used. For instance, spray coating can achieve a uniform pore distribution, but it may result in nonuniform catalyst loading and poor CL-membrane interphase, which in turn compromises the overall performance.[110,111] By contrast, slot-die/microgroove coating ensures better catalyst distribution for large-scale manufacturing and improves the interface quality.[112] Sputter coating on PTL, as a porous transport electrode, can reduce precious metal use and eliminate ionomers, thereby enhancing durability and kinetics by reducing ionomer-related degradation.[113] Thus, every coating method has its advantages; a more effective approach would be to adapt the coating process by controlling the CL microstructure.

5.2. Ir-supported catalysts

Advanced support materials with high conductivity, high surface area and higher corrosion-resistance could increase the catalyst utilization and maintain catalyst integrity through

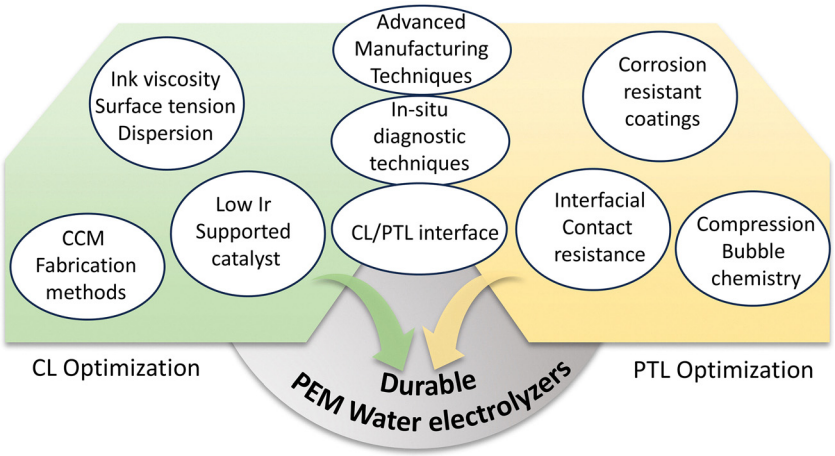

Fig. 8 Schematics illustration of proposed strategies to improve the performance and durability of CL and PTL.

strong metal–support interaction.[114] Nanostructured Ir-supported catalysts significantly improve catalyst utilization through a higher electrochemically active surface area.[115] Similarly, conductive supports improve charge transfer and electrical conductivity within the CL and aid in improving the OER kinetics. More importantly, the corrosion resistant catalyst support inhibits the Ir nanoparticles detachment and retain the catalytic performance over long term stability testing.[25] Nanostructural design of low Ir supported catalyst also provides efficient mass transport properties due to optimized porosity and pore size distribution by balancing the water/gas transport and reduces mechanical stress.[116] Additionally, optimizing the CL morphology by controlling thickness, porosity, and the ionomer interface improves proton conductivity and reduces degradation.[19]

5.3. Corrosion-resistant coating

The surface passivation forms a non-conductive oxide layer, which negatively impacts PTL conductivity, resulting in higher cell voltages. These phenomena could be mitigated through noble metal coatings that inhibit the PTL corrosion.[117] Currently, PTL is coated with Pt (200 nm thick layer) to prevent surface passivation; however, it increases the cost per kilogram of H_2 generated and makes the total process more expensive. Using an interlayer between the Ti-based substrate and the Pt top layer can reduce Pt loading by up to four times without sacrificing performance.[73] Corrosion-resistant and low-cost metals such as tantalum and niobium, which as more noble than Ti but less noble than Pt, act as an electrochemical buffer. These interlayers could reduce the potential difference between Ti and Pt, thereby inhibiting the interfacial corrosion and improve long-term stability.[73]

5.4. Interfacial contact resistance

The significant variation in particle size of the CL and PTL such as the nanometer size of catalyst nanoparticles in the CL causes inadequate interfacial contact between PTL (micrometer size particles) and CL. Insufficient contact leads to low charge transfer efficiency. The interfacial contact could be enhanced by adding a mesoporous layer on top of PTL. For instance, a laser ablation modified Ti at PTL–CL interface with a uniform microporous backing layer, offers scalable and efficient method for PTL fabrication.[118] This structural refinement enhances the mass transport and catalyst utilization in PEMWEs, enabling superior performance at low Ir loadings without compromising interfacial integrity. Similarly, a proper compression during assembly plays a crucial role in interfacial contact resistance, *i.e.*, inadequate or excessive compression significantly impacts the HFR values, which lead to higher voltage losses. Optimized compression is also crucial for preventing mechanical damage while maintaining effective water and gas transport. Thus, it is essential to perform compression testing for proper compression validation before testing the cell performance.

5.5. *In situ* diagnostic

Recent developments in *in situ* analysis techniques have brought useful information about CL and PTL degradations at early stages. For instance, the bubble detachment is a severe issue that disrupts the PTL microstructure and leads to PTL degradation during long term testing. Transparent designs of CL/PTL system with *in situ* visualizations can track the microstructural changes in CL/PTL, bubble dynamics over the course of time.[108] Thus, by *in situ* visualization, the bubble detachment could be improved by smart design of PTL microstructure and its wettability. Similarly, some methods such as vibrations or ultrasonic waves could also be utilized to mitigate the bubble induced structural degradation of PTL. *In situ* durability evaluation is also useful to study the dynamic process happening at the CL/PTL interface. For instance, coupling durability studies with advanced operando techniques such as EIS and spatial ICR mapping, synchrotron/neutron imaging, or XAS/XPS can directly link transient electrochemical signals to oxide growth, bubble dynamics, and interfacial chemical changes. Visual summaries that align load profiles with electrochemical response and structural/morphological evolution provide a

powerful way to interpret how dynamic operation accelerates PTL degradation and propagates failure into the CL and membrane. Further developments in *in situ* monitoring and real-time diagnostics for both CL and PTL could enable the early detection of degradation towards targeted interventions. These approaches can help to identify performance losses at an early stage and enable the support predictive maintenance for extended operational lifetime of PEMWEs.

5.6. Durability protocols

Overall limitations in the testing framework to isolate degradation of individual components makes it difficult to compare the published results. However, future durability studies in PEMWEs should prioritize stressor-specific testing protocols to isolate degradation mechanisms more effectively. Literature shows that constant high-current operation accelerates irreversible losses due to Ti-PTL passivation and catalyst contamination, while dynamic cycling helps distinguish reversible degradation. Furthermore, OCV-based ASTs uniquely identify IrOx transformation and contact resistance buildup. These findings highlight the need for tailored protocols: varying in current density, cycling frequency, and voltage holds, to decouple mechanical, electrochemical, and material degradation for next generation electrolyzer design. For PTL, the half-cell testing and *ex situ* corrosion experiments allow the evaluation of PTL passivation, coating stability. Similarly, ICR measurements under controlled compression can identify mechanical or chemical degradation related to oxide growth and surface roughening. Dynamic potential cycling mimic renewable energy-driven load fluctuations, reproducing transient stresses that accelerate passivation and interfacial degradation. Although these methods provide useful insights, the establishment of harmonized and component-specific durability test procedures remains an important priority for the PEMWE community.

5.7. Advanced manufacturing techniques

The manufacturing methods are aimed to lower (PGM) loading through controlled deposition which include magnetron sputter and reactive spray deposition technology. The CCMs from magnetron sputtering usually exhibit superior electrochemical activity and improved durability. However, this method is suitable for supported catalyst only, as un-supported IrOx catalyst results in a thinner CL, which is vulnerable to early-stage mechanical degradation.[119] Likewise, reactive spray deposition technology could potentially open a new pathway in fabricating a CL with low PGM loading for extended applications in PEMWEs ($\sim$5000 h). However, dissolution of Ir from the anode CL still prevails and results in migration of Ir into membrane, re-deposition at cathode and Oxidation to form IrO_2.[120] While these new CL fabrication techniques show a promising result, they are only operated at current densities below 2 A cm^{-2} at laboratory scale. These studies exhibit an early-stage implications of technology scaling up for industrial applications. In parallel, emerging manufacturing techniques for durable and functional PTLs include additive manufacturing and controlled powder sintering, which allow fine tuning of pore-size gradients and tortuosity to optimize gas transport and interfacial contact. Furthermore, laser surface structuring, magnetron sputtering, and atomic layer deposition facilitate precise control of surface morphology and chemical composition, improving corrosion resistance and reducing contact resistance under dynamic operation. Integrating these advanced fabrication techniques with standardized durability testing will be crucial for developing next-generation PTLs that exhibit both long-term stability and enhanced electrochemical performance.

6. Conclusion

CL and PTL form the backbone of PEMWEs, shaping both their performance, durability and cost. To extend the lifetime and reducing the overall cost of next generation PEMWEs, it is crucial to understand how these components degrade and find smarter ways to protect them. The CL performance could be improved by optimizing catalyst inks composition and methods, designing stable Ir-supported catalysts for better catalyst utilization through controlled microstructural engineering. The PTL durability can be enhanced through corrosion-resistant coatings, improved interfacial contact with the CL, and microstructural designs that mitigate passivation and mechanical degradation. *In situ* and operando diagnostics are also essential to track degradation pathways and establish correlations between electrochemical behavior and structural changes. These innovations would make it possible to use less precious metal for a lower cost and move closer to sustainable and affordable green hydrogen production.

Conflicts of interest

There are no conflicts to declare.

Abbreviations

AEMWE	Anion exchange membrane water electrolyzer
AST	Accelerated stress test
AWE	Alkaline water electrolyzer
BOT	Beginning of test
CL	Catalyst layer
CV	Cyclic voltammetry
ECSA	Electrochemical surface area
EDS	Energy dispersive X-ray spectroscopy
EIS	Electrochemical impedance spectroscopy
EOT	End of test
HER	Hydrogen evolution reaction
HFR	High frequency resistance
ICR	Interfacial contact resistance
MEA	Membrane electrode assembly
OER	Oxygen evolution reaction
PEMWE	Proton exchange membrane water electrolyzer
PGM	Platinum group metal

PTL	Porous transport layer
SEM	Scanning electron microscopy
SOEC	Solid oxide electrolyzer cell
TEM	Transmission electron microscopy
XPS	X-ray photoelectron spectroscopy
XRD	X-ray diffraction

Data availability

No new data were created or analyzed in this study. Data sharing is not applicable to this article.

Acknowledgements

We would like to acknowledge the support of the Natural Sciences and Engineering Research Council of Canada (NSERC), Canada Research Chair (CRC-2019-00354), Discovery grant (CRSNG-DGECR-2022-00058) and Mitacs Accelerate (IT25281).

References

1 T. Terlouw, C. Bauer, R. McKenna and M. Mazzotti, Large-scale hydrogen production via water electrolysis: a techno-economic and environmental assessment, *Energy Environ. Sci.*, 2022, **15**, 3583–3602.
2 N. Dubouis, D. Aymé-Perrot, D. Degoulange, A. Grimaud and H. Girault, Alkaline electrolyzers: Powering industries and overcoming fundamental challenges, *Joule*, 2024, **8**, 883–898.
3 T. Wang, X. Cao and L. Jiao, PEM water electrolysis for hydrogen production: fundamentals, advances, and prospects, *Carb. Neutrality.*, 2022, **1**, 21.
4 F. Gutiérrez-Martín, L. Amodio and M. Pagano, Hydrogen production by water electrolysis and off-grid solar PV, *Int. J. Hydrogen Energy*, 2021, **46**, 29038–29048.
5 R. T. Liu, Z. L. Xu, F. M. Li, F. Y. Chen, J. Y. Yu, Y. Yan, Y. Chen and B. Y. Xia, Recent advances in proton exchange membrane water electrolysis, *Chem. Soc. Rev.*, 2023, **52**, 5652–5683.
6 H. Cheng, H. Luo, J. Cheng, W. Hao, J. Song and G. Xu, Optimizing the corrosion resistance of additive manufacturing TC4 titanium alloy in proton exchange membrane water electrolysis anodic environment, *Int. J. Hydrogen Energy*, 2024, **93**, 753–769.
7 H. B. Tao, H. Liu, K. Lao, Y. Pan, Y. Tao, L. Wen and N. Zheng, The gap between academic research on proton exchange membrane water electrolysers and industrial demands, *Nat. Nanotechnol.*, 2024, **19**, 1074–1076.
8 S. Hao, H. Sheng, M. Liu, J. Huang, G. Zheng, F. Zhang, X. Liu, Z. Su, J. Hu, Y. Qian, L. Zhou, Y. He, B. Song, L. Lei, X. Zhang and S. Jin, Torsion strained iridium oxide for efficient acidic water oxidation in proton exchange membrane electrolyzers, *Nat. Nanotechnol.*, 2021, **16**, 1371–1377.
9 M. Rogler, R. Wagner, S. Thiele and M. Suermann, Guidance for targeted degradation analysis of OER kinetics of low-loading iridium-based catalysts in PEM water electrolysis cells, *Electrochim. Acta*, 2025, **510**, 145360.
10 S. Shiva Kumar and V. Himabindu, Hydrogen production by PEM water electrolysis – A review, *Mater. Sci. Energy Technol.*, 2019, **2**, 442–454.
11 J. O. M. Bockris, Kinetics of activation controlled consecutive electrochemical reactions: anodic evolution of oxygen, *J. Chem. Phys.*, 1956, **24**, 817–827.
12 Z. W. Seh, J. Kibsgaard, C. F. Dickens, I. Chorkendorff, J. K. Nørskov and T. F. Jaramillo, Combining theory and experiment in electrocatalysis: Insights into materials design, *Science*, 2017, **355**, eaad4998.
13 H. Ren, X. Meng, Y. Lin and Z. Shao, Microstructure formation mechanism of catalyst layer and its effect on fuel cell performance: Effect of dispersion medium composition, *J. Energy Chem.*, 2022, **73**, 588–598.
14 N. Todoroki, R. Kudo, K. Hayashi, M. Yokoi, N. Naraki and T. Wadayama, Improving the oxygen evolution activity and stability of Nb-doped TiO_2-supported RuO_2 by a SnO_2 interlayer: A model catalyst study on single-crystal oxide heterostructures, *ACS Catal.*, 2023, **13**, 11433–11440.
15 Y. Duan, L. L. Wang, W. X. Zheng, X. L. Zhang, X. R. Wang, G. J. Feng, Z. Y. Yu and T. B. Lu, Oxyanion engineering on RuO_2 for efficient proton exchange membrane water electrolysis, *Angew. Chem., Int. Ed.*, 2024, **63**, e202413653.
16 C. Spori, J. T. H. Kwan, A. Bonakdarpour, D. P. Wilkinson and P. Strasser, The stability challenges of oxygen evolving catalysts: Towards a common fundamental understanding and mitigation of catalyst degradation, *Angew. Chem., Int. Ed.*, 2017, **56**, 5994–6021.
17 L. An, C. Wei, M. Lu, H. Liu, Y. Chen, G. G. Scherer, A. C. Fisher, P. Xi, Z. J. Xu and C. H. Yan, Recent Development of Oxygen Evolution Electrocatalysts in Acidic Environment, *Adv. Mater.*, 2021, **33**, e2006328.
18 S. Cherevko, S. Geiger, O. Kasian, A. Mingers and K. J. J. Mayrhofer, Oxygen evolution activity and stability of iridium in acidic media. Part 2. – Electrochemically grown hydrous iridium oxide, *J. Electroanal. Chem.*, 2016, **774**, 102–110.
19 E. Padgett, H. Yu, S. J. Blair, D. Cullen, R. K. Ahluwalia, D. J. Myers, B. Pivovar and S. M. Alia, Quantifying Sources of Voltage Decay in Long-Term Durability Testing for PEM Water Electrolysis, *J. Electrochem. Soc.*, 2025, **172**, 054508.
20 O. Kasian, J.-P. Grote, S. Geiger, S. Cherevko and K. J. J. Mayrhofer, The Common Intermediates of Oxygen Evolution and Dissolution Reactions during Water Electrolysis on Iridium, *Angew. Chem., Int. Ed.*, 2018, **57**, 2488–2491.
21 S. M. Alia, B. Rasimick, C. Ngo, K. C. Neyerlin, S. S. Kocha, S. Pylypenko, H. Xu and B. S. Pivovar, Activity and durability of iridium nanoparticles in the oxygen evolution reaction, *J. Electrochem. Soc.*, 2016, **163**, F3105–F3112.
22 O. Kasian, J. P. Grote, S. Geiger, S. Cherevko and K. J. J. Mayrhofer, The common intermediates of oxygen

evolution and dissolution reactions during water electrolysis on Iridium, *Angew. Chem., Int. Ed.*, 2018, **57**, 2488–2491.

23 Q. Feng, X. Z. Yuan, G. Liu, B. Wei, Z. Zhang, H. Li and H. Wang, A review of proton exchange membrane water electrolysis on degradation mechanisms and mitigation strategies, *J. Power Sources*, 2017, **366**, 33–55.

24 H. Yu, L. Bonville, J. Jankovic and R. Maric, Microscopic insights on the degradation of a PEM water electrolyzer with ultra-low catalyst loading, *Appl. Catal., B*, 2020, **260**, 118194.

25 Z. Shi, J. Li, J. Jiang, Y. Wang, X. Wang, Y. Li, L. Yang, Y. Chu, J. Bai, J. Yang, J. Ni, Y. Wang, L. Zhang, Z. Jiang, C. Liu, J. Ge and W. Xing, Enhanced acidic water oxidation by dynamic migration of oxygen species at the Ir/Nb_2O_{5-x} catalyst/support interfaces, *Angew. Chem., Int. Ed.*, 2022, **61**, e202212341.

26 S. Zaman, M. Khalid and S. Shahgaldi, Advanced electrocatalyst supports for proton exchange membrane water electrolyzers, *ACS Energy Lett.*, 2024, 2922–2935.

27 D. Hoffmeister, S. Finger, L. Fiedler, T. C. Ma, A. Korner, M. Zlatar, B. Fritsch, K. W. Bodnar, S. Carl, A. Gotz, B. A. Zubiri, J. Will, E. Spiecker, S. Cherevko, A. T. S. Freiberg, K. J. J. Mayrhofer, S. Thiele, A. Hutzler and C. van Pham, Photodeposition-based synthesis of TiO_2@IrOx core-shell catalyst for proton exchange membrane water electrolysis with low Iridium loading, *Adv. Sci.*, 2024, **11**, e2402991.

28 C. V. Pham, M. Bühler, J. Knöppel, M. Bierling, D. Seeberger, D. Escalera-López, K. J. J. Mayrhofer, S. Cherevko and S. Thiele, IrO_2 coated TiO_2 core-shell microparticles advance performance of low loading proton exchange membrane water electrolyzers, *Appl. Catal., B*, 2020, **269**, 117862.

29 C. Daiane Ferreira da Silva, F. Claudel, V. Martin, R. Chattot, S. Abbou, K. Kumar, I. Jiménez-Morales, S. Cavaliere, D. Jones, J. Rozière, L. Solà-Hernandez, C. Beauger, M. Faustini, J. Peron, B. Gilles, T. Encinas, L. Piccolo, F. H. Barros de Lima, L. Dubau and F. Maillard, Oxygen Evolution Reaction Activity and Stability Benchmarks for Supported and Unsupported IrOx Electrocatalysts, *ACS Catal.*, 2021, **11**, 4107–4116.

30 Y. Wang, M. Zhang, Z. Kang, L. Shi, Y. Shen, B. Tian, Y. Zou, H. Chen and X. Zou, Nano-metal diborides-supported anode catalyst with strongly coupled TaO_x/IrO_2 catalytic layer for low-iridium-loading proton exchange membrane electrolyzer, *Nat. Commun.*, 2023, **14**, 5119.

31 T. S. Wenjuan Shi, C. Xing, K. Sun, Q. Yan, W. Niu, X. Yang, J. Li, C. Wei, R. Wang, S. Fu, Y. Yang, L. Xue, J. Chen, S. Cui, X. Hu, K. Xie, X. Xu, S. Duan, Y. Xu and B. Zhang, Ultrastable supported oxygen evolution electrocatalyst formed by ripening-induced embedding, *Science*, 2025, **387**, 791–796.

32 S. Yuan, C. Zhao, X. Cai, L. An, S. Shen, X. Yan and J. Zhang, Bubble evolution and transport in PEM water electrolysis: Mechanism, impact, and management, *Prog. Energy Combust. Sci.*, 2023, **96**, 101075.

33 H. Liu, Y. Yang, J. Liu, M. Huang, K. Lao, Y. Pan, X. Wang, T. Hu, L. Wen, S. Xu, S. Li, X. Fang, W. F. Lin, N. Zheng and H. B. Tao, Constructing Robust 3D Ionomer Networks in the Catalyst Layer to Achieve Stable Water Electrolysis for Green Hydrogen Production, *ACS Appl. Mater. Interfaces*, 2024, **16**, 16408–16417.

34 Z. Xie, H. Chen, X. Wang, Y. A. Wu, Z. Wang, S. Jana, Y. Zou, X. Liang, X. Zhao and X. Zou, Honeycomb-Structured IrOx Foam Platelets as the Building Block of Anode Catalyst Layer in PEM Water Electrolyzer, *Angew. Chem., Int. Ed.*, 2024, e202415032.

35 Y. Wang, Z. Zhao, X. Liang, X. Zhao, X. Wang, S. Jana, Y. A. Wu, Y. Zou, L. Li, H. Chen and X. Zou, Supported IrO(2) Nanocatalyst with Multilayered Structure for Proton Exchange Membrane Water Electrolysis, *Adv. Mater.*, 2024, **36**, e2407717.

36 Z. Xie, L. Xiao, K. Zhenye, Z. Yongcun, W. Xiyang, W. Yimin A., K. Graham, L. Qi, H. Yalan, Z. Xiao, C. Hui, Z. Xiaoxin and F. Jiao, High-Porosity, Layered Iridium Oxide as an Efficient, Durable Anode Catalyst for Water Splitting, *CCS Chem*, 2025, **7**, 216–228.

37 S. Xu, H. Liu, N. Zheng and H. B. Tao, Physical Degradation of Anode Catalyst Layer in Proton Exchange Membrane Water Electrolysis, *Adv. Mater. Interfaces*, 2024, **1**, 2400549.

38 E. Wallnöfer-Ogris, I. Grimmer, M. Ranz, M. Höglinger, S. Kartusch, J. Rauh, M.-G. Macherhammer, B. Grabner and A. Trattner, A review on understanding and identifying degradation mechanisms in PEM water electrolysis cells: Insights for stack application, development, and research, *Int. J. Hydrogen Energy*, 2024, **65**, 381–397.

39 S. H. Frensch, F. Fouda-Onana, G. Serre, D. Thoby, S. S. Araya and S. K. Kær, Influence of the operation mode on PEM water electrolysis degradation, *Int. J. Hydrogen Energy*, 2019, **44**, 29889–29898.

40 G. Wei, Y. Wang, C. Huang, Q. Gao, Z. Wang and L. Xu, The stability of MEA in SPE water electrolysis for hydrogen production, *Int. J. Hydrogen Energy*, 2010, **35**, 3951–3957.

41 H. Yu, N. Danilovic, Y. Wang, W. Willis, A. Poozhikunnath, L. Bonville, C. Capuano, K. Ayers and R. Maric, Nano-size IrOx catalyst of high activity and stability in PEM water electrolyzer with ultra-low iridium loading, *Appl. Catal., B.*, 2018, **239**, 133–146.

42 A. Z. Tomić, I. Pivac and F. Barbir, A review of testing procedures for proton exchange membrane electrolyzer degradation, *J. Power Sources*, 2023, **557**, 232569.

43 F. Hegge, F. Lombeck, E. Cruz Ortiz, L. Bohn, M. von Holst, M. Kroschel, J. Hübner, M. Breitwieser, P. Strasser and S. Vierrath, Efficient and Stable Low Iridium Loaded Anodes for PEM Water Electrolysis Made Possible by Nanofiber Interlayers, *ACS Appl. Energy Mater.*, 2020, **3**, 8276–8284.

44 H. Sayed-Ahmed, Á. I. Toldy and A. Santasalo-Aarnio, Dynamic operation of proton exchange membrane electrolyzers—Critical review, *Renewable Sustainable Energ Rev.*, 2024, **189**, 113883.

45 S. Yuan, C. Zhao, X. Cai, L. An, S. Shen, X. Yan and J. Zhang, Bubble evolution and transport in PEM water electrolysis: Mechanism, impact, and management, *Prog. Energy Combust. Sci.*, 2023, **96**, 101075.
46 A. Gupta, Y. M. Chellehbari and S. Shahgaldi, Achieving high performance and durability with ultra-low precious metal nanolayer on porous transport layer for PEMWE application, *J. Power Sources*, 2025, **630**, 236088.
47 F. Zeng, C. Mebrahtu, L. Liao, A. K. Beine and R. Palkovits, Stability and deactivation of OER electrocatalysts: A review, *J. Energy Chem.*, 2022, **69**, 301–329.
48 Y. He, S. Feng, H. Chen, Y. Liu, X. Shi, P. Rao, J. Li, X. Wu, S. Huang, K. Li, H. Wang, X. Tian and Z. Kang, Direct kinetic loss analysis with hierarchy configuration of catalyst coated membrane in proton exchange membrane water electrolysis cell, *Fuel*, 2025, 379.
49 O. Panchenko, M. Carmo, M. Rasinski, T. Arlt, I. Manke, M. Müller and W. Lehnert, Non-destructive in-operando investigation of catalyst layer degradation for water electrolyzers using synchrotron radiography, *Mater. Today Energy.*, 2020, **16**, 100394.
50 A. Weiß, A. Siebel, M. Bernt, T. H. Shen, V. Tileli and H. A. Gasteiger, Impact of intermittent operation on lifetime and performance of a PEM water electrolyzer, *J. Electrochem. Soc.*, 2019, **166**, F487–F497.
51 M. Möckl, M. F. Ernst, M. Kornherr, F. Allebrod, M. Bernt, J. Byrknes, C. Eickes, C. Gebauer, A. Moskovtseva and H. A. Gasteiger, Durability testing of low-Iridium PEM water electrolysis membrane electrode assemblies, *J. Electrochem. Soc.*, 2022, **169**, 064505.
52 S. M. Alia, K. S. Reeves, D. A. Cullen, H. Yu, A. J. Kropf, N. Kariuki, J. H. Park and D. J. Myers, Simulated Start-Stop and the Impact of Catalyst Layer Redox on Degradation and Performance Loss in Low-Temperature Electrolysis, *J. Electrochem. Soc.*, 2024, 171.
53 S. M. Alia and G. C. Anderson, Iridium oxygen evolution activity and durability baselines in rotating disk electrode half-cells, *J. Electrochem. Soc.*, 2019, **166**, F282–F294.
54 F. M. Li, L. Huang, S. Zaman, W. Guo, H. Liu, X. Guo and B. Y. Xia, Corrosion Chemistry of Electrocatalysts, *Adv. Mater.*, 2022, **34**, e2200840.
55 S. M. Alia, S. Stariha and R. L. Borup, Electrolyzer durability at low catalyst loading and with dynamic operation, *J. Electrochem. Soc.*, 2019, **166**, 1164.
56 C. Rakousky, U. Reimer, K. Wippermann, M. Carmo, W. Lueke and D. Stolten, An analysis of degradation phenomena in polymer electrolyte membrane water electrolysis, *J. Power Sources*, 2016, **326**, 120–128.
57 C. Rakousky, U. Reimer, K. Wippermann, S. Kuhri, M. Carmo, W. Lueke and D. Stolten, Polymer electrolyte membrane water electrolysis: Restraining degradation in the presence of fluctuating power, *J. Power Sources*, 2017, **342**, 38–47.
58 C. Liu, M. Shviro, G. Bender, A. S. Gago, T. Morawietz, M. J. Dzara, I. Biswas, P. Gazdzicki, Z. Kang, S. F. Zaccarine, S. Pylypenko, K. A. Friedrich, M. Carmo and W. Lehnert, Degradation effects at the porous transport layer/catalyst layer interface in polymer electrolyte membrane water electrolyzer, *J. Electrochem. Soc.*, 2023, 170.
59 S. F. Zaccarine, M. Shviro, J. N. Weker, M. J. Dzara, J. Foster, M. Carmo and S. Pylypenko, Multi-scale multi-technique characterization approach for analysis of PEM electrolyzer catalyst layer degradation, *J. Electrochem. Soc.*, 2022, **169**, 064502.
60 F. Claudel, L. Dubau, G. Berthomé, L. Sola-Hernandez, C. Beauger, L. Piccolo and F. Maillard, Degradation Mechanisms of Oxygen Evolution Reaction Electrocatalysts: A Combined Identical-Location Transmission Electron Microscopy and X-ray Photoelectron Spectroscopy Study, *ACS Catal.*, 2019, **9**, 4688–4698.
61 Z. Taie, X. Peng, D. Kulkarni, I. V. Zenyuk, A. Z. Weber, C. Hagen and N. Danilovic, Pathway to Complete Energy Sector Decarbonization with Available Iridium Resources using Ultralow Loaded Water Electrolyzers, *ACS Appl. Mater. Interfaces*, 2020, **12**, 52701–52712.
62 A. S. Pushkarev, I. V. Pushkareva, M. A. Solovyev, M. Prokop, T. Bystron, S. K. Rajagopalan, K. Bouzek and S. A. Grigoriev, On the influence of porous transport layers parameters on the performances of polymer electrolyte membrane water electrolysis cells, *Electrochim. Acta*, 2021, **399**, 139436.
63 L. Moradizadeh, P. V. Madhavan, A. Ozden, X. Li and S. Shahgaldi, Advances in protective coatings for porous transport layers in proton exchange membrane water electrolyzers: Performance and durability insights, *Energy Convers. Manage.*, 2025, **332**, 119713.
64 T. Bystron, M. Vesely, M. Paidar, G. Papakonstantinou, K. Sundmacher, B. Bensmann, R. Hanke-Rauschenbach and K. Bouzek, Enhancing PEM water electrolysis efficiency by reducing the extent of Ti gas diffusion layer passivation, *J. Appl. Electrochem.*, 2018, **48**, 713–723.
65 C. Liu, M. Shviro, A. S. Gago, S. F. Zaccarine, G. Bender, P. Gazdzicki, T. Morawietz, I. Biswas, M. Rasinski, A. Everwand, R. Schierholz, J. Pfeilsticker, M. Müller, P. P. Lopes, R. A. Eichel, B. Pivovar, S. Pylypenko, K. A. Friedrich, W. Lehnert and M. Carmo, Exploring the interface of skin-Layered itanium fibers for electrochemical water splitting, *Adv. Energy Mater.*, 2021, **11**, 2002926.
66 T. Bautkinova, N. Utsch, T. Bystron, M. Lhotka, M. Kohoutkova, M. Shviro and K. Bouzek, Introducing titanium hydride on porous transport layer for more energy efficient water electrolysis with proton exchange membrane, *J. Power Sources*, 2023, **565**, 232913.
67 C. Rakousky, U. Reimer, K. Wippermann, M. Carmo, W. Lueke and D. Stolten, An analysis of degradation phenomena in polymer electrolyte membrane water electrolysis, *J. Power Sources*, 2016, **326**, 120–128.
68 B. Hasa, U. R. Aryal, S. Higashi, N. E. Tolouei, J. T. Lang, B. Erb, A. Smeltz, I. V. Zenyuk and G. Zhu, Porous transport layer influence on overpotentials in PEM water electrolysis at low anode catalyst loadings, *Appl. Catal., B*, 2025, **361**, 124616.

69 M. Prestat, Corrosion of structural components of proton exchange membrane water electrolyzer anodes: A review, *J. Power Sources*, 2023, **556**, 232469.
70 P. V. Madhavan, L. Moradizadeh, S. Shahgaldi and X. Li, Data-Driven Modelling of Corrosion Behaviour in Coated Porous Transport Layers for PEM Water Electrolyzers, *Artif. Intell. Chem.*, 2025, 100086.
71 C. Liu, M. Carmo, G. Bender, A. Everwand, T. Lickert, J. L. Young, T. Smolinka, D. Stolten and W. Lehnert, Performance enhancement of PEM electrolyzers through iridium-coated titanium porous transport layers, *Electrochem. Commun.*, 2018, **97**, 96–99.
72 L. Moradizadeh, P. V. Madhavan, Y. M. Chellehbari, A. Gupta, X. Li and S. Shahgaldi, Porous transport layers with low Pt loading having Nb–Ta alloy as interlayer for proton exchange membrane water electrolyzers, *Int. J. Hydrogen Energy*, 2024, **94**, 1114–1129.
73 L. Moradizadeh, M. Johar, Y. M. Chellehbari, X. Li and S. Shahgaldi, Optimized tantalum interlayer thickness for PTLs: Enhancing PEMWE performance, stability, and reducing precious metal loading, *J. Power Sources*, 2025, **647**, 237360.
74 A. Tan, Y. Zhang, X. Shi, C. Ju, P. Liu, T. Yang and J. Liu, The poisoning effects of Ti-ion from porous transport layers on the membrane electrode assembly of proton exchange membrane water electrolyzers, *Chem. Eng. J.*, 2023, **471**, 144624.
75 T. Kadyk, D. Bruce and M. Eikerling, How to enhance gas removal from porous electrodes?, *Sci. Rep.*, 2016, **6**, 38780.
76 E. Leonard, A. D. Shum, S. Normile, D. C. Sabarirajan, D. G. Yared, X. Xiao and I. V. Zenyuk, Operando X-ray tomography and sub-second radiography for characterizing transport in polymer electrolyte membrane electrolyzer, *Electrochim. Acta*, 2018, **276**, 424–433.
77 M. Suermann, T. J. Schmidt and F. N. Büchi, Investigation of mass transport losses in polymer electrolyte electrolysis cells, *ECS Trans.*, 2015, **69**, 1141.
78 S. A. Grigoriev, P. Millet, S. A. Volobuev and V. N. Fateev, Optimization of porous current collectors for PEM water electrolysers, *Int. J. Hydrogen Energy*, 2009, **34**, 4968–4973.
79 X.-Z. Yuan, N. Shaigan, C. Song, M. Aujla, V. Neburchilov, J. T. H. Kwan, D. P. Wilkinson, A. Bazylak and K. Fatih, The porous transport layer in proton exchange membrane water electrolysis: perspectives on a complex component, *Sustainable Energy Fuels*, 2022, **6**, 1824–1853.
80 A. Voronova, S. Kim, D. Kim, H.-Y. Park, J. H. Jang and B. Seo, Systematic degradation analysis in renewable energy-powered proton exchange membrane water electrolysis, *Energy Environ. Sci.*, 2023, **16**, 5170–5184.
81 P. Millet, A. Ranjbari, F. de Guglielmo, S. A. Grigoriev and F. Auprêtre, Cell failure mechanisms in PEM water electrolyzers, *Int. J. Hydrogen Energy*, 2012, **37**, 17478–17487.
82 M. Wang, Z. Wang and Z. Guo, Water electrolysis enhanced by super gravity field for hydrogen production, *Int. J. Hydrogen Energy*, 2010, **35**, 3198–3205.
83 D. Zhu, L. Xu, X. Su, B. Hu, T. Jia and L. Mi, Experimental study of the effect of mechanical vibration and water velocity on bubble management in PEM electrolysis cell, *Int. J. Hydrogen Energy*, 2024, **49**, 390–403.
84 H. Li, T. Fujigaya, H. Nakajima, A. Inada and K. Ito, Optimum structural properties for an anode current collector used in a polymer electrolyte membrane water electrolyzer operated at the boiling point of water, *J. Power Sources*, 2016, **332**, 16–23.
85 K. Shigemasa, K. Wani, T. Nakayama, K. Watanabe, K. Wakuda, R. Shiono, K. Asaoka, T. Araki, K. Nagasawa and S. Mitsushima, Effects of porous transport layer wettability on performance of proton exchange membrane water electrolyzer: Mass transport overvoltage and visualization of oxygen bubble dynamics with high-speed camera, *Int. J. Hydrogen Energy*, 2024, **62**, 601–609.
86 T. Schuler, T. J. Schmidt and F. N. Büchi, Polymer electrolyte water electrolysis: correlating performance and porous transport layer structure: Part II. Electrochemical Performance Analysis, *J. Electrochem. Soc.*, 2019, **166**, F555.
87 Nitta, O. Himanen and M. Mikkola, Thermal Conductivity and Contact Resistance of Compressed Gas Diffusion Layer of PEM Fuel Cell, *Fuel Cells*, 2008, **8**, 111–119.
88 F. Lapicque, M. Belhadj, C. Bonnet, J. Pauchet and Y. Thomas, A critical review on gas diffusion micro and macroporous layers degradations for improved membrane fuel cell durability, *J. Power Sources*, 2016, **336**, 40–53.
89 P. Lettenmeier, S. Kolb, F. Burggraf, A. S. Gago and K. A. Friedrich, Towards developing a backing layer for proton exchange membrane electrolyzers, *J. Power Sources*, 2016, **311**, 153–158.
90 P. Lettenmeier, R. Wang, R. Abouatallah, B. Saruhan, O. Freitag, P. Gazdzicki, T. Morawietz, R. Hiesgen, A. S. Gago and K. A. Friedrich, Low-cost and durable bipolar plates for proton exchange membrane electrolyzers, *Sci. Rep.*, 2017, **7**, 44035.
91 X. Gao, T. Huang, P. Tang, J. Di, L. Zhong and W. Zhang, Enhancing scanning electron microscopy imaging quality of weakly conductive samples through unsupervised learning, *Sci. Rep.*, 2024, **14**, 6439.
92 J. Mo, S. M. Steen, F.-Y. Zhang, T. J. Toops, M. P. Brady and J. B. Green, Electrochemical investigation of stainless steel corrosion in a proton exchange membrane electrolyzer cell, *Int. J. Hydrogen Energy*, 2015, **40**, 12506–12511.
93 A. V. Lubenchenko, A. A. Batrakov, A. B. Pavolotsky, O. I. Lubenchenko and D. A. Ivanov, XPS study of multilayer multicomponent films, *Appl. Surf. Sci.*, 2018, **427**, 711–721.
94 T. Greunz, R. Steinberger, B. Strauß and D. Stifter, Reduction of hexavalent chromium embedded in organic insulation and corrosion inhibition layers during X-ray photoelectron spectroscopy (XPS) measurements, *Corros. Sci.*, 2018, **143**, 39–45.
95 A. P. Black, A. Sorrentino, F. Fauth, I. Yousef, L. Simonelli, C. Frontera, A. Ponrouch, D. Tonti and M. R. Palacin,

Synchrotron radiation based operando characterization of battery materials, *Chem. Sci.*, 2023, **14**, 1641–1665.

96 U. Panchenko, T. Arlt, I. Manke, M. Müller, D. Stolten and W. Lehnert, Synchrotron Radiography for a Proton Exchange Membrane (PEM) Electrolyzer, *Fuel Cells*, 2020, **20**, 300–306.

97 M. Zlobinski, T. Schuler, F. N. Büchi, T. J. Schmidt and P. Boillat, Transient and Steady State Two-Phase Flow in Anodic Porous Transport Layer of Proton Exchange Membrane Water Electrolyzer, *J. Electrochem. Soc.*, 2020, **167**, 084509.

98 W. Wang, S. Yu, K. Li, L. Ding, Z. Xie, Y. Li, G. Yang, D. A. Cullen, H. Yu, Z. Kang, J. A. Wrubel, Z. Ma, G. Bender, C. B. Capuano, A. Keane and F.-Y. Zhang, Insights into the rapid two-phase transport dynamics in different structured porous transport layers of water electrolyzers through high-speed visualization, *J. Power Sources*, 2021, **516**, 230641.

99 Z. Kang, J. Mo, G. Yang, Y. Li, D. A. Talley, S. T. Retterer, D. A. Cullen, T. J. Toops, M. P. Brady, G. Bender, B. S. Pivovar, J. B. Green and F.-Y. Zhang, Thin film surface modifications of thin/tunable liquid/gas diffusion layers for high-efficiency proton exchange membrane electrolyzer cells, *Appl. Energy*, 2017, **206**, 983–990.

100 C. Liu, K. Wippermann, M. Rasinski, Y. Suo, M. Shviro, M. Carmo and W. Lehnert, Constructing a multifunctional interface between membrane and porous transport layer for water electrolyzers, *ACS Appl. Mater. Interfaces*, 2021, **13**, 16182–16196.

101 S. Stiber, H. Balzer, A. Wierhake, F. J. Wirkert, J. Roth, U. Rost, M. Brodmann, J. K. Lee, A. Bazylak, W. Waiblinger, A. S. Gago and K. A. Friedrich, Porous transport layers for proton exchange membrane electrolysis under extreme conditions of current density, temperature, and pressure, *Adv. Energy Mater.*, 2021, **11**, 2100630.

102 A. Z. Tomić, I. Pivac and F. Barbir, A review of testing procedures for proton exchange membrane electrolyzer degradation, *J. Power Sources*, 2023, **557**, 232569.

103 A. Voronova, S. Kim, D. Kim, H.-Y. Park, J. H. Jang and B. Seo, Systematic degradation analysis in renewable energy-powered proton exchange membrane water electrolysis, *Energy Environ. Sci.*, 2023, **16**, 5170–5184.

104 X. Shi, X. Qiu, Z. Yuan, R. Zhang, K. Zhao, A. Tan, G. Xu, J. Song and J. Liu, Effects of the Dynamic Loading Frequency on Performance of the Proton Exchange Membrane Water Electrolysis, *ACS Appl. Mater. Interfaces*, 2024, **16**, 66089–66098.

105 C. C. Weber, J. A. Wrubel, L. Gubler, G. Bender, S. De Angelis and F. N. Buchi, How the porous transport layer interface affects catalyst utilization and performance in polymer electrolyte water electrolysis, *ACS Appl. Mater. Interfaces*, 2023, **15**, 34750–34763.

106 C. C. Weber, S. De Angelis, R. Meinert, C. Appel, M. Holler, M. Guizar-Sicairos, L. Gubler and F. N. Büchi, Microporous transport layers facilitating low iridium loadings in polymer electrolyte water electrolysis, *EES Catal.*, 2024, **2**, 585–602.

107 M. Kroschel, A. Bonakdarpour, J. T. H. Kwan, P. Strasser and D. P. Wilkinson, Analysis of oxygen evolving catalyst coated membranes with different current collectors using a new modified rotating disk electrode technique, *Electrochim. Acta*, 2019, **317**, 722–736.

108 S. Yu, K. Li, W. Wang, Z. Xie, L. Ding, Z. Kang, J. Wrubel, Z. Ma, G. Bender, H. Yu, J. Baxter, D. A. Cullen, A. Keane, K. Ayers, C. B. Capuano and F. Y. Zhang, Tuning Catalyst Activation and Utilization Via Controlled Electrode Patterning for Low-Loading and High-Efficiency Water Electrolyzers, *Small*, 2022, **18**, e2107745.

109 T. Bautkinova, M. Prokop, T. Bystron and K. Bouzek, Interface between anode porous transport layer and catalyst layer: A key to efficient, stable and competitive proton exchange membrane water electrolysis, *Curr. Opin. Electrochem.*, 2025, **49**, 101624.

110 R. Liu, W. Zhou, L. Wan, P. Zhang, S. Li, Y. Gao, D. Xu, C. Zheng and M. Shang, Electrostatic spraying of membrane electrode for proton exchange membrane fuel cell, *Curr. Appl. Phys.*, 2020, **20**, 11–17.

111 S. M. Alia, K. S. Reeves, J. S. Baxter and D. A. Cullen, The impact of ink and spray variables on catalyst layer properties, electrolyzer performance, and electrolyzer durability, *J. Electrochem. Soc.*, 2020, **167**, 144512.

112 J. Park, Z. Kang, G. Bender, M. Ulsh and S. A. Mauger, Roll-to-roll production of catalyst coated membranes for low-temperature electrolyzers, *J. Power Sources*, 2020, **479**, 228819.

113 J. K. Lee, G. Anderson, A. W. Tricker, F. Babbe, A. Madan, D. A. Cullen, J. D. Arregui-Mena, N. Danilovic, R. Mukundan, A. Z. Weber and X. Peng, Ionomer-free and recyclable porous-transport electrode for high-performing proton-exchange-membrane water electrolysis, *Nat. Commun.*, 2023, **14**, 4592.

114 C. Lee, K. Shin, Y. Park, Y. H. Yun, G. Doo, G. H. Jung, M. Kim, W. C. Cho, C. H. Kim, H. M. Lee, H. Y. Kim, S. Lee, G. Henkelman and H. S. Cho, Catalyst-Support Interactions in Zr2ON2-Supported IrOx Electrocatalysts to Break the Trade-Off Relationship Between the Activity and Stability in the Acidic Oxygen Evolution Reaction, *Adv. Funct. Mater.*, 2023, **33**, 2301557.

115 L. Moriau, M. Smiljanic, A. Loncar and N. Hodnik, Supported iridium-based oxygen evolution reaction electrocatalysts - recent developments, *ChemCatChem*, 2022, **14**, e202200586.

116 S. Zaman, M. Wang, H. Liu, F. Sun, Y. Yu, J. Shui, M. Chen and H. Wang, Carbon-based catalyst supports for oxygen reduction in proton-exchange membrane fuel cells, *Trends Chem.*, 2022, **4**, 886.

117 S. Singh, A. Singh, M. A. Iqbal and S. Shahgaldi, Constructing an ultra-low loading of IrPt bimetallic coated porous transport layer (PTL) for a PEM water electrolyzer application, *Int. J. Hydrogen Energy*, 2025, **157**, 150478.

118 J. K. Lee, T. Schuler, G. Bender, M. Sabharwal, X. Peng, A. Z. Weber and N. Danilovic, Interfacial engineering via

laser ablation for high-performing PEM water electrolysis, *Appl. Energy*, 2023, **336**, 120853.
119 T. Hrbek, P. Kúš, Y. Kosto, M. G. Rodríguez and I. Matolínová, Magnetron-sputtered thin-film catalyst with low-Ir-Ru content for water electrolysis: Long-term stability and degradation analysis, *J. Power Sources*, 2023, **556**, 232375.
120 Z. Zeng, R. Ouimet, L. Bonville, A. Niedzwiecki, C. Capuano, K. Ayers, A. P. Soleymani, J. Jankovic, H. Yu, G. Mirshekari, R. Maric and S. Bliznakov, Degradation Mechanisms in Advanced MEAs for PEM Water Electrolyzers Fabricated by Reactive Spray Deposition Technology, *J. Electrochem. Soc.*, 2022, **169**, 054536.